Examensarbete
TVVR 07/5007

Monitoring of Incomati River Basin with Remote Sensing

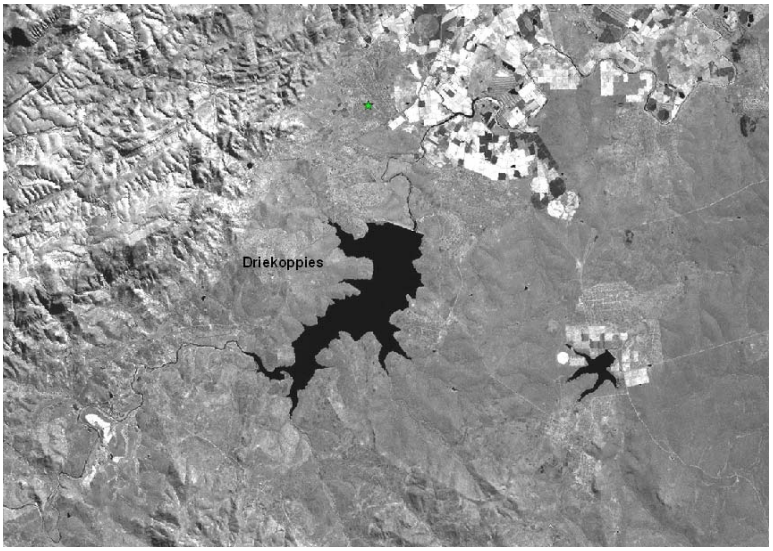

Bijan Khalili

May 2007

Division of Water Resources Engineering
Department of Building and Environmental Technology
Lund University

Avdelning för Teknisk Vattenresurslära
ISRN LUTVDG/TVVR - 07/5007+57p
ISSN-1101-9824

Monitoring of Incomati River Basin with Remote Sensing

Division of Water Resources Engineering
Department of Building and Environmental Technology
Lund University, Sweden

May 2007

Supervisors:
- Dr. Rolf Larsson: Department of Water Resources Engineering,
Lund Institute of Technology (LTH), Lund University, Sweden
- Prof. dr. ir. Nick van de Giesen: Department of Water Resources Management, Faculty of Civil Engineering and Geosciences,
Delft University of Technology (TUD), the Netherlands

Examiner: Professor Magnus Larson

Master Thesis by: Bijan Khalili

Picture on front page:
Water surface in Driekoppies dam stands out in complete contrast with its surrounding. Landsat image band 4 taken on 2001-5-30

May 2007
Report TVVR 07/5007
Master of Science Thesis in Water Resources
Division of Water Resources
Lund Institute of Technology, Lund University
Box 118 SE - 221 00 Lund
Sweden
Phone: +46 46 2220000
Web Address: http://aqua.tvrl.lth.se

Abstract

Incomati river basin is located in the continent of South Africa and is shared between three countries of Republic of Mozambique, Republic of South Africa, and the Kingdom of Swaziland. Located in a water-stressed region and shared between three countries it has importance in both sociopolitical and water scarcity aspect. The three countries recently (in 2002) signed an agreement for letting certain amount of water pass through the borders. Accordingly all 3 countries need to implement a monitoring method to evaluate the agreement. This thesis deals with different remote sensing methods for monitoring of water resources in the basin. To do this, after explaining site conditions, different literature has been reviewed and three main remote sensing methods (Optical method, Synthetic Aperture Radar imagery (SAR), Radar Altimetry) are explained briefly. Their advantages and disadvantages and their limitations are discussed. By creating an inventory of available satellites and considering the site specific conditions the use and applicability of those methods to the region are discussed. This paper shows that among the three major Remote Sensing methods, optical method and Synthetic Aperture Radar (SAR) can be used for monitoring of the Incomati basin.

Furthermore, the optical method was applied to assess water storage in the region. Some free Landsat images of the region obtained from Global Land Cover Facility (GLCF), www.landcover.org have been analyzed and water storage has been estimated and the results compared with ground truth information. The results obtained from 6 Landsat images showed high accuracy of water storage estimation with an average accuracy of 3.5%.

Acknowledgement

- Landsat images used in this project have been obtained from the Global Land Cover Facility (GLCF), www.landcover.org.
- I am indebted to my supervisors Dr. Rolf Larsson at department of Water Resources Engineering, Lund Institute of Technology(LTH), Lund University, Sweden and Prof. dr. ir. Nick van de Giesen at Water Resources Management department of the Faculty of Civil Engineering and Geosciences, Delft University of Technology (TUD), the Netherlands. Their knowledge, advices, critical comments, supports, encouragement and their patience, helped me to gain more knowledge and to have a more fruitful thesis work.
- I am again indebted to Prof. dr. ir. Nick van de Giesen at TUDelft, for accepting me and letting me go to the Water Resources Management department, TUD. I gained many things during that period and it was a very fruitful travel for me and my thesis.
- Thanks to Dr. Lennart Jönsson for helping me to have a good start in my thesis and for introducing me useful related references.
- Thanks to my examiner, Professor Magnus Larson, for his academic advice and corrections.
- Thanks to my dear parents, who encouraged me and supported me in all part of my life and especially for their encouragements and supports for furthering my education.
- Thanks to the Department of Water Affairs and Forestry - South Africa (DWAF) for providing the related information
- Lastly, thanks to all my friends, family and classmates who have in some way supported and encouraged me.

Table of contents

List of figures

List of tables

Abbreviations, Acronyms, and Symbols

ASTER	The Advanced Spaceborne Thermal Emission and Reflection Radiometer
CC	Cloud Coverage
CNES	Centre National d' ´ Etudes Spatiales
DEOS	Delft Institute for Earth-Oriented Space Research
DWAF	Department of Water Affairs and Forestry - South Africa
EOS	Earth Observing System (EOS)
ERS	European Remote Sensing satellite
ESA	European Space Agency
GDR	Geophysical Data Records
GFO	Geosat Follow-On satellite
GIS	Geographical Information Systems
HH	Horizontal-Horizontal (polarization)
IGDR, MGDR, RGDR	Interim/Merged/Real-time Geophysical Data Records
M.a.s.l	Mean Average Sea Level
MSS	Mean Sea Surface
NASA	National Aeronautics and Space Administration
POD	Precise Orbit Determination
RADS	Radar Altimeter Database System
RS	Remote Sensing
SAR	Synthetic Aperture Radar
SSH	Sea Surface Height
SWH	Significant Wave Height
TIR	Thermal InfRared
TOPEX	Topography Experiment satellite
USGS	United States Geological Survey
VNIR	Visible and Near-InfRared
VV	Vertical-Vertical (polarization)

1 Background

1.1 Site description

Incomati river basin is one of the international river basins located in the southeast corner of Africa (Figure 1). It covers an area of about 46,700 km^2 and is shared between Republic of Mozambique, Republic of South Africa, and the Kingdom of Swaziland.

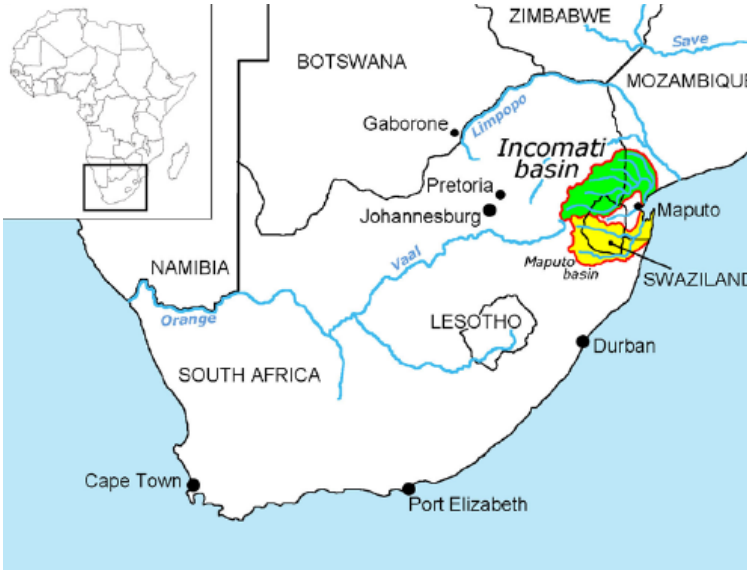

Figure 1- The Incomati Basin in southern Africa (Source: Carmo Vaz and Van der Zaag, 2003)

Even though Incomati is a relatively small basin, it is of strategic importance, because it is located in an area of intense development pressure, which results in a considerably high demand for its water resources (Almeida, 2004). This importance of the catchment can be discussed in both socio-political developments and water scarcity.

The Incomati river rises from the west of the basin and the eastern part of South Africa in the mountains of approximately 2000 meter height (above sea level).Then it flows from the eastern part of South Africa, through the north of Swaziland and drops to the coastal plain to the east of the Lebombo mountains at elevations below 150 m. Finally it flows into the southern part of Mozambique where it discharges into the Indian Ocean in Maputo Bay. The two adjacent basins of Umbeluzi and Maputo basins, which are also shared by the three countries, both discharge in to Maputo Bay. Figure 2 shows the contribution of the area of the three countries in this basin.

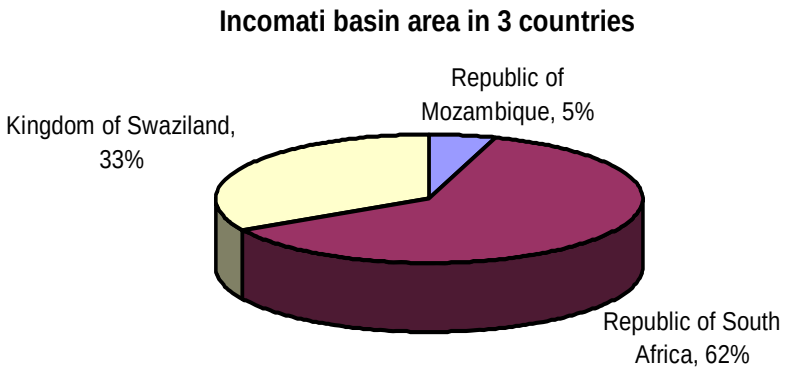

Figure 2 - Coverage of Incomati catchment area in different countries.

(Adapted from information in Almeida 2004 cited from JIBS, 2001)

As figure 3 shows, The Incomati river has 6 main tributary rivers, namely the the Komati, Crocodile, Sabie, Massintonto, Uanetze and Mazimechopes. The total length of the Komati River from its source to the confluence with the Crocodile River is approximately 450 km (NKomo et al 2003). Geology of basin is characterized by sedimentary, volcanic, granitic, and dolomitic rocks, and quarternary and recent deposits (Carmo Vaz and Van der Zaag, 2003).

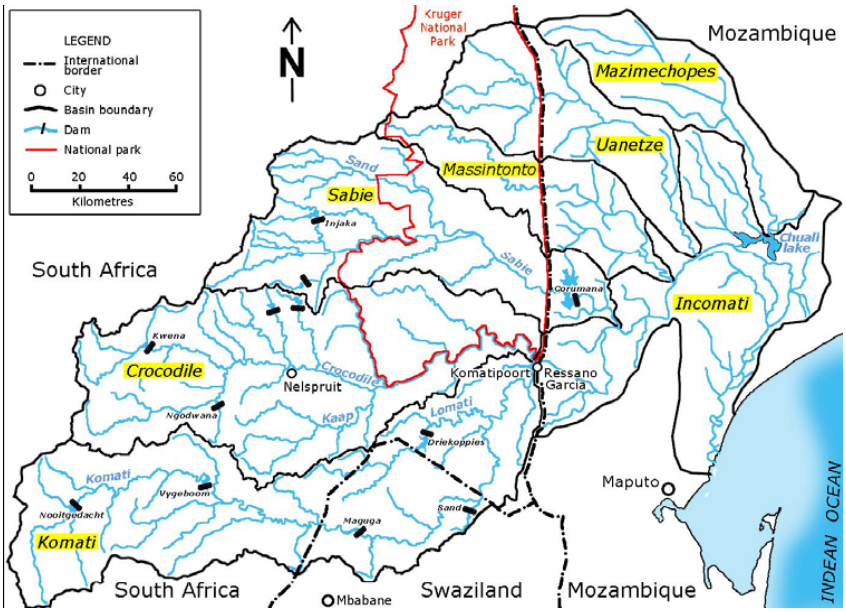

Figure 3 - The Incomati basin and its catchment areas (Source:Carmo Vaz and Van der Zaag, 2003)

1.2 Climate

The general climate in the Incomati river basin varies from a warm to hot humid climate in the Mozambique coastal plain and the Lowveld to a cooler dry climate in the Transvaal Plateau and South African Highveld in the west (Carmo Vaz and Van der Zaag, 2003).
The Incomati river basin lies entirely within the summer rainfall region (October–March). Mean annual precipitation of the region is about 740 mm/a. The mean annual potential evaporation for the basin is about 1,900 mm/a (Almeida 2004). Rainfall increases from east to west and the potential evaporation decreases from east to west hence irrigation becomes more important for crop production towards the east. The deficit between rainfall and potential evaporation illustrates the importance of suitable water management in the catchment.

1.3 Hydrology

The Joint Incomati Basin Study (JIBS), undertaken in 2001, estimated the net virgin runoff of the Incomati river basin at 77 mm/year (3,590 Mm^3/a) (Almeida 2004). Virgin or natural runoff is the runoff that would occur if the catchment was in a completely natural state, neglecting the effect of development in the catchment. Table 1 shows the summary of runoff generation.

In the year 2002 the estimated total consumptive water use was about 1,800 Mm^3/a, including consumptive use of exotic forest plantations (Carmo Vaz and Van der Zaag, 2003).
Therefore the total estimated water consumptive represents about 50 percent of the virgin runoff. Given the high variability of flow, both within and between years, this level of commitment is high and frequently leads to water shortage (Elmeida 2004).

Table 1 - Water generation in the Incomati Basin, by catchment

(Source: cited in Carmo Vaz and Van der Zaag, 2003 from JIBS, 2001)

Catchment	Catchment area Mm2	Virgin discharge	
		Mm3/a	mm/a
Komati	11,209	1,420	127
Crocodile	10,468	1,226	117
Sabie	7,048	750	106
Massintonto	3,429	22	6
Uanetze	3,932	14	4
Mazimechopes	3,970	21	5
Incomati	6,692	134	20
Total	46,748	3,587	77

1.4 Water usage

The Incomati catchment has several water consumers, some of which can be in conflict with one another. The major part of water is used for irrigation, forest plantation, domestic and municipal water use, industrial use, inter-basin transfers and environmental water demands. These uses have resulted in the commitment of a large percentage of the catchment's mean annual runoff (Nkomo and van der Zaag, 2003). This level of commitment is high, and according to high variability of flow, frequently leads to water shortages. During the wet years, there will be enough water in the catchment. In dry years, however, there may not be enough water stored. In such years, arguments between the treaty members states may easily arise, which would undermine regional cooperation and sustainable development.

1.5 Major reservoirs

Because of high demand of water and according to high variability of flow, large dams have been constructed. As table 2 shows, presently, there are 8 major dams constructed in the Incomati catchment, with a total storage capacity of about 2,000 Mm^3. In addition to these major dams, the catchment contains some smaller farm dams and weirs.

Table 2 – Major dams in the Incomati catchment (adapted from data in Carmo Vaz and Van der Zaag, 2003 and DWAF)

No.	Reservoir name	Country	Tributary	Storage (Mm^3)	Year *	Latitude	Longitide
1	Corumana dam	Mozambique	Sabie	879	1988	-25.12	32.06
2	Maguga dam	Swaziland	Komati	332	2002	-26.1	31.3
3	Driekoppies dam	South Africa	Lomati	251	1998	-25.7	31.5
4	Kwena dam	South Africa	Crocodile	155	1984	-25.3	30.4
5	Injaka dam	South Africa	Sabie	120	2001	-24.9	31.1
6	Vygeboom dam	South Africa	Komati	84	1971	-25.9	30.6
7	Nooitgedacht dam	South Africa	Komati	81	1962	-26.0	30.1
8	Sand River dam	Swaziland	Komati	49	1966	-26.0	31.7

** Year: Commissioned Year*

1.6 Water related conflict and cooperation

Frequently, debate has arisen between users and riparian countries. Downstream farmers have often complained about interbasin transfers taking place in the upstream portions of the catchment (Nkomo et al 2003). Despite historical differences and differing economic conditions, the three riparian countries agreed upon a Tripartite Interim Agreement (TIA) on the sustainable utilization of the water resources of the Incomati and Maputo watercourses. Water usage and demands are stated in the Tripartite Interim Agreement (TIA) signed in Johannesburg in 2002. The treaty foresees letting certain amounts of water pass the borders to satisfy the needs of downstream neighbors.

2 Objective

The purpose of this M.Sc. thesis is to evaluate the use of remote sensing technique as a tool, enabling all member states to agree upon the state of water availability.
After literature review, it tries to do a feasibility study for the three main Remote Sensing (RS) methods:

- Optical methods
- Synthetic Aperture Radar (SAR)
- Radar Altimetry (RA)

For this evaluation, temporal and spatial resolution of the abovementioned methods should be discussed. The existing hurdles and sources of errors should be explained and accuracy of the methods should be estimated. Finally the thesis suggests the required specification for each method to give a reasonable result.

3 Methods

3.1 Overview

Schultz et al (2000) defined Remote Sensing (RS) as the science and art of obtaining information about an object, area, or phenomenon through the analysis of data acquired by a sensor that is not in direct contact with the target of investigation (Cited in Schultz et al 2000 from Ritchie and Rango, 1996). In a very simple way even using our eyes to read or look at any object is also a form of remote sensing. However, remote sensing includes not only what is visual, but also what can't be seen with the eyes, including sound and heat. Remote sensing can be conducted on different platforms like aircraft, satellites, balloons, probes, etc containing different instruments.

Remote sensing normally uses measurements of the electromagnetic spectrum to characterize the landscape and its properties. Schultz et al (2000) mentioned that, while using RS, hydrological parameters are usually not measured directly. Generally some interpretation is required to convert RS data to hydrologically relevant information.

Traditionally, in-situ gauging networks have been installed for several decades to measure hydrological parameters like water levels and discharge rates. In some cases due to geographical, political or economical limitations, gauges are scarce or even absent in parts of basins. For certain major rivers and wetlands, hydrological information can often be difficult to obtain due to a region's inaccessibility, the sparse distribution of gauge stations, or the slow dissemination of data (Birkett 1998). In these cases alternative methods like RS can be used instead.

Recently, remote sensing techniques have been used to monitor hydrological parameters on time scales ranging from months to decades. Nowadays earth observation technologies and Geographical Information Systems (GIS) are beginning to play a greater role in the development of the water resources management.
Remote sensing and its continued development have added new techniques that hydrologists can use in a large number of applications. The choice of which satellite system to use depends upon the requirements for the data, which translate into the need for specific spectral bands, spatial requirements, temporal coverage, and the possible need for stereo coverage, all of which are related to the satellite platform (Schultz et al 2000).

Here the three main Remote Sensing (RS) methods are explained and discussed:
- Optical methods
- Synthetic Aperture Radar (SAR) imagery
- Radar Altimetry (RA)

Using the first two methods, one can detect a water surface and calculate its area. Later the water volume can be calculated based on the relationship between water surface and water storage in a known reservoir. The last method (RA) can be used to directly measure the water level.

Many projects, including evaluation of water resources and flood mapping, require data of the extent of water bodies. The detection of water bodies is a concern that has been pursued since the first LANDSAT images became available in 1972 (Barber et al. 1996).
The repetitive and synoptic nature of satellite remotely sensed data allow monitoring of water bodies over large regions of land. Remote Sensing (RS) data in both the optical and the microwave region of the electromagnetic (EM) spectrum has been used for water body delineation and discrimination of it from surrounding land.

3.2 Optical Method

3.2.1 Overview

Since Landsat data became available in 1972, researchers started to use optical methods (passive images) for water body detection and delineation. Water absorbs most energy in the near and middle infrared wavelengths (>0.8 μm), so there is little energy available for reflection at these wavelengths. As figure 4 shows, in the optical range (visible – infrared) water has a distinctively low spectral response. The other materials like soil and healthy vegetation have higher reflectance in these spectral bands. Thus, on grayscale images of these bands or on multi-spectral scanner images in the reflective infra-red portion of the spectrum, water bodies appear dark and stand out in complete contrast to surrounding vegetative and soil features (Schultz et al 2000) which allows good delineation between water and its surrounding.

Therefore, locating and delineating surface waters can be most easily done using remotely sensed data in the near-infrared and visible wavelengths.

Based on a previous study of Engman & Gurney (1991) and Figure 4, Schultz et al. (2000) concluded that water has a low reflectivity in the wavebands between 0.7 and 3.0 μm. This region of the spectrum is quite effective for water surface delineation.

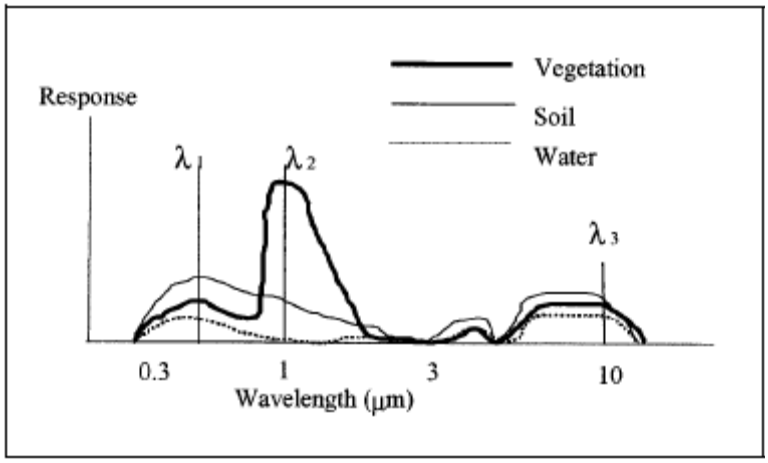

Figure 4 - Reflectance vs. wavelength for soil, vegetation and water

(Source: Schultz et al. - 2000, adapted from Swain and Davis 1978)

Schultz et al. (2000) showed that this region of the spectrum aligns itself well with different bands of major satellites. Table 3, summarizes this alignment. Many studies have shown the effectiveness of these wavelengths for mapping open water regions. In many studies Landsat data (TM and MSS) or SPOT data have been used to determine the extent of water bodies using simple classification procedures, usually with an infrared band. Figure 5 (right side) shows the complete contrast between water and its surrounding in Landsat ETM band 4 and compare it with that in Landsat ETM band 2 (left side)of the same region acquired the same day.

Table 3 - Suitable bands of Landsat, SPOT and NOAA AVHR for water delineation,

(Adapted from info. in Schultz et al. - 2000)

Satellite/ Instrument	Band	Wavelength (μm)
Landsat MSS	7	0.8-1.1
Landsat TM	4	0.76-0.90
SPOT-HRV	3	0.79 – 0.89
NOAA AVHRR	2	0.72 – 1.1

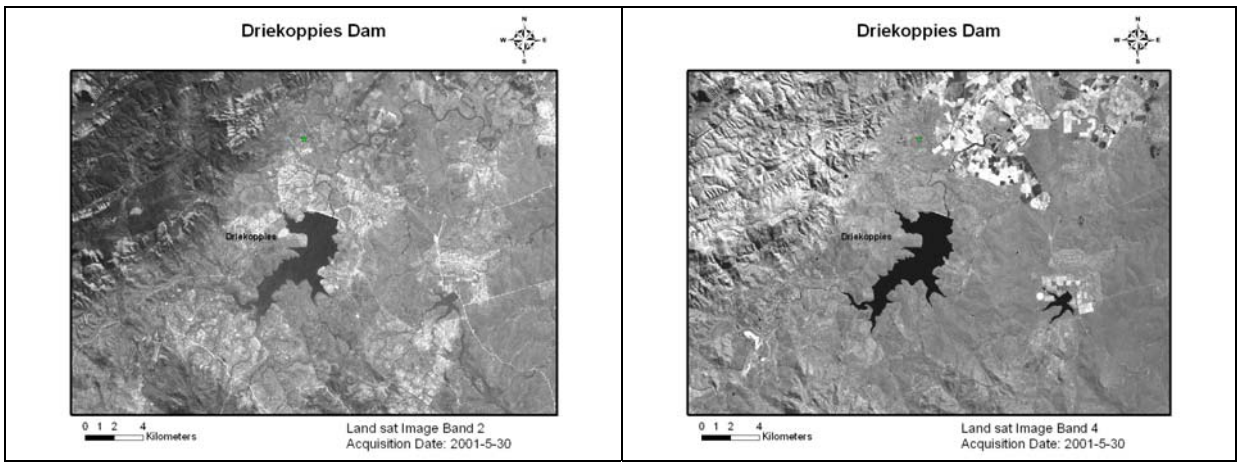

Figure 5 - Driekopies Dam; The water body stands in complete contrast with its surrounding in Landsat ETM+ band 4 (right) but not in the Landsat ETM+ band 2 (left). (Image acquired on: 2001-5-30)

3.2.2 Nature of wave reflectance

As Figure 6 shows, the spectral reflectance pattern from water bodies is composed of three influencing parameters (Liebe, 2002):

- Surface reflection: Surface reflection is influenced by the sun-sensor- constellations and the roughness of water surface created by wind (Liebe, 2002). Under calm conditions, the reflection might be specular, while surface waves and certain sun-to-sensor constellations cause less specular reflection and more diffusion instead. Standing and floating vegetation alters the reflectance properties of a water body by adding a "red edge" to the return signal (Mather 1999).
- Volume reflection: The volume reflection influences the signal due to turbidity, dissolved matter, the tropic status and algae content of the reservoir water (Liebe, 2002). The amount of contribution of volume reflection to the total reflection signal of a water body depends on the penetration depth of light which depends on wavelength. The penetration depth of light depends on the wavelength. It is about 10 m in the 0.5 – 0.6 μm waveband and less than 10 cm in the 0.8 – 1.1 μm range (cited from MEIJERINK et all. 1994 in Liebe, 2002).
- Bottom reflection: Bottom reflection, is another component of reflection. Shorter wavelength penetrates deeper in the water and so they contribute more in reflection from bottom.

Figure 6 - Processes acting on solar radiant energy in the visible part of the spectrum over an area of shallow water.

(Source: Mather 1999)

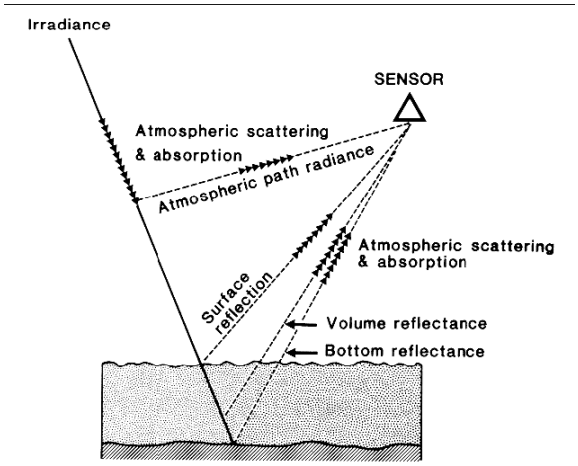

Generally many parameters, including presence and concentration of dissolved and suspended organic and inorganic material, turbidity, water depth, floating vegetation and algae contents affect the reflectance of a water body and cause spectral variation in water. Figure 7 shows different reflectance pattern of water bodies.

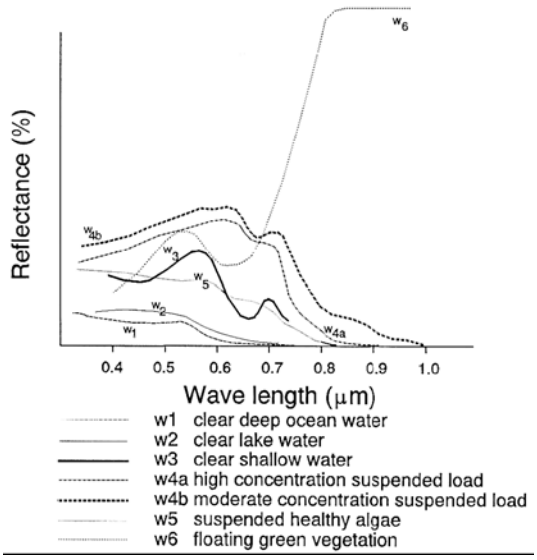

Figure 7 - Possible reflectance curves of water bodies (relative reflectance).

(Source: Liebe 2000, cited from MEIJERINK et al. 1994)

3.2.3 Sources of errors & hurdles

- Clouds: A major disadvantage of optical imagery is its vulnerability to cloud cover. Asner (2001) considers clouds as a major obstacle to optical remote sensing of humid tropical regions, and recommended a cloud cover probability analysis.

- Sun-glint: In certain sun-to-sensor constellations, "Sun-glint" phenomena may cause misinterpretation of optical images. Sun-glint is the reflection of the sun off the surface of calm water that causes the water body to appear white (or lighter than normal tone) instead of black (Figure 8). In places, where the solar angles are relatively low, like Alaska and Australia, the sun-glint is more pronounced. But according to the location of the study region, this problem may not occur in this case study.

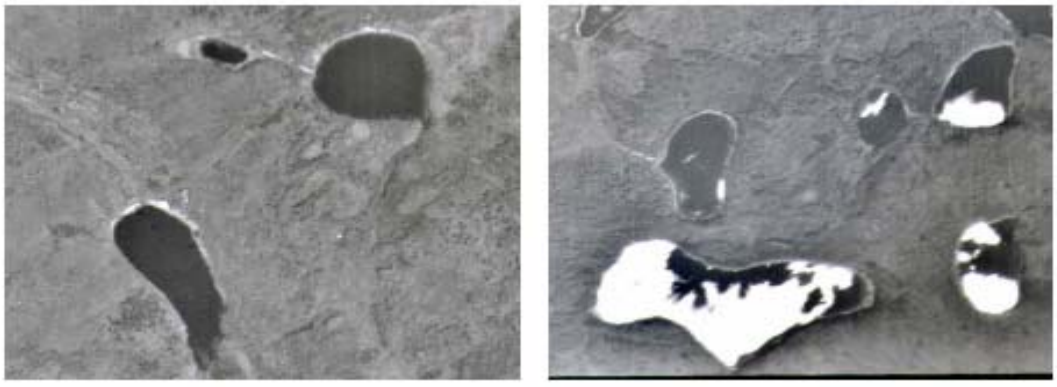

Figure 8 - Example of water bodies without (left) and with (right) sun-glint. Sun-glint causes a water body to appear white (Source: Riordan, 2005).

- Spectral overlap: There might be some spectral overlap between the brightness values found in water and its surrounding area. For example very moist or waterlogged soil areas surrounding water may have spectral overlap with water and classify as water. This can be one source of error which overestimates the water surface.

- Floating vegetation: Floating vegetation, algal blooms, or emerging vegetation on top or closely surrounding a water body might lead to misclassification during the water body identification stage. This will lead to an underestimation of the water surface. To account for this, some measures should be considered. For example Riordan 2005, in his case study toggled the bands displayed from band 5 to color infrared, where vegetation becomes more apparent. By observing a water body in both band 5 and CIR, he was able to establish the water body borders more accurately.

Liebe, 2002 in his case study of Ghana had similar results. In his results, some of the reservoir areas were bigger than that from remote sensing, giving fluctuation in the accuracies. Based on the on site data, he explained occurrence of carpet of floating herbaceous vegetation and other herbaceous water plants cover in the water surface as a major source of this error. Later he added that densely vegetation covered water surfaces were not classified as water during the satellite image classification and caused misclassification. Liebe 2002 cited from BALSER (1996), that multisensor data fusion, e.g. of Landsat with ERS (Radar)- Imagery is a useful solution to this special condition.

3.3 Synthetic Aperture Radar (SAR)

3.3.1 Overview

Microwave remote sensing platforms can also be used for surface water delineation, since they are sensitive to water discrimination and in the meantime they have the distinct advantage of functioning in nearly all-weather conditions. Generally water reflects most of the incidence wave in a specular way (Figure 9-Left), while the surrounding land surface usually behaves as a diffuse reflector, providing a return signal to the satellite (Figure 9-Right). Active sensors such as ERS-1 and 2, JERS-1 and Radarsat have all shown potential for estimating open water boundaries because of the specular reflection of the incident wave and very low return at the operating angels of these satellites (Schultz et al. - 2000). Some parameters affect the efficiency of radar images, which is discussed below.

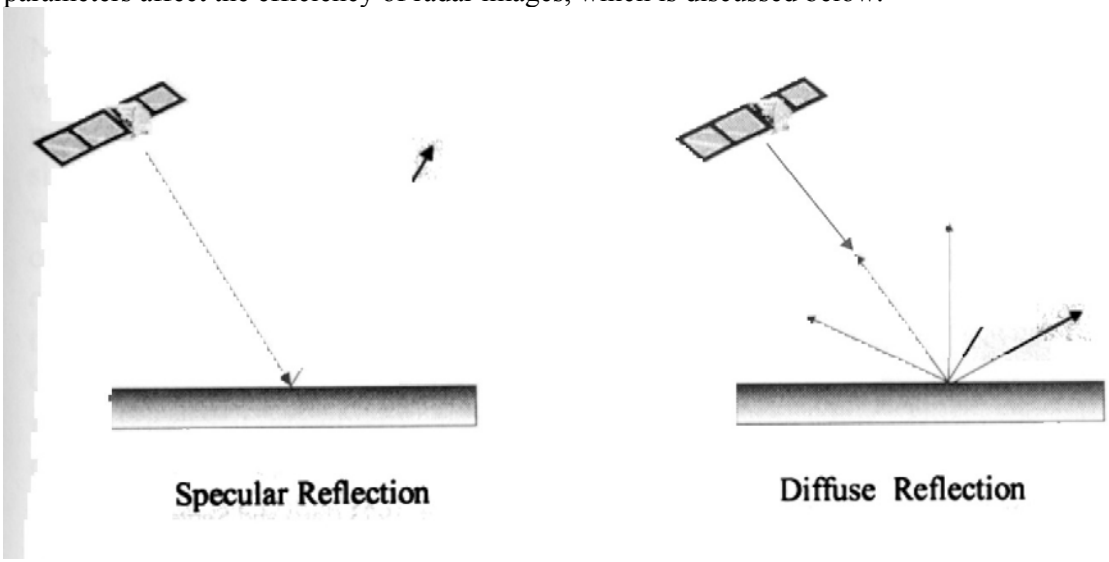

Figure 9 - Specular reflection – Diffusal reflection (Source: Schultz et al. - 2000)

3.3.2 Incidence angle

The large incidence angle range (θ = 45 to 76 degree) causes most of the energy to be scattered in the specular direction, resulting in a small scattering coefficient (σ^o) or dark tone (Barber et al. - 1996). This will create more contrast between water and its surrounding and will ease the water surface delineation.

At low incidence angles, the water surface can be subjected to Bragg resonance effects where the incident pulse responds to the short ripples or waves which increases the backscatter response from an open water target. In general X and C-Band receivers are sensitive to centimeter surface waves while L-Band radars are sensitive to decimeter surface wave heights (Schultz et al. - 2000).
Schultz et al. (2000) recommended large incidence angles for surface water delineation.

Barber et al. 1996, in a case study of flood mapping at Manitoba of Canada showed that ERS-1 data do not provide nearly as detailed a boundary between the flooded and non-flooded areas as due primarily to the shallow angle of incidence (θ = 23). The shallow angle of incidence and small-scale surface roughness caused much of the energy to be scattered back to the ERS-1 platform instead of being scattered in a specular way. They concluded that high incidence angles (greater than 45 degree) works better than low incidence angles for delineating of flood boundaries with SAR.

3.3.3 Polarization

Polarization is another factor affecting the radar backscatter. Barber et al. (1996), in a case study of flood mapping at Manitoba of Canada showed that vertical-vertical (VV) polarized signal on the ERS satellites is much more sensitive to surface wind and waves than the same frequency horizontal-horizontal (HH) signal onboard the Radarsat satellite. They cited from Ulaby et al. (1986) that VV polarizations are more susceptible to small-scale surface roughness in water bodies than is HH polarization.

3.4 Image processing

In order to use remote sensing imagery data, one has to analyze and interpret satellite images to extract meaningful data. This can be done within image processing procedures. Image processing involves four different main stages:

1- Pre - processing: Pre-processing involves the operations that usually are necessary to be applied on images before any further process. This includes geometric and radiometric corrections. Radiometric corrections may be necessary due to variations in scene illumination, atmospheric conditions, and sensor noise and response. Generally, data obtained in different occasions or obtained from different sensors have different illuminations. To compare these data it is better to have similar illumination and so pre-processing is necessary.

2- Image Enhancement: Image Enhancement is the process for improvement of appearance of the images to have easier visual interpretation. This enhancement includes adjustment of the range and distribution of brightness values and can be done in different ways like contrast changes, changes in the tone of image and applying of different filters to highlight some pattern of interest or highlight certain features of scene. Most remote sensing devices pass over a diverse range of targets during their missions including water, snowfields, desert, etc. and so they receive a large spectral response variation. They are designed to cope with several different levels of target/background energy in a routine base. According to diversity of spectral responses no generic radiometric correction can be applied. Thus, for each application, a custom image enhancement should be done to have optimum brightness range and contrast for the targets of interest.

3- Image Transformation: Image transformation typically consists of the manipulation of multiple sources of data to generate "new" images to highlight a particular feature of interest. The sources of data can be different bands obtained from a single multispectral image or from different images of the same area acquired at different times. Basic image transformations use simple arithmetic operations to the image data. Image subtraction is one example of arithmetic operations that can be used to identify changes that have occurred between images collected on different dates.

4- Image classification and Analysis: The objective of classification is to assign image pixels to particular classes or themes like water, forest, crops,… based on statistical characteristics of the pixel brightness values. While working with GIS, one dealt with two different types of classes: information classes and spectral classes. Information classes are the actual categories that the analyst is trying to identify in the imagery, such as water bodies, different geological units or different kinds of crops, etc…. Spectral classes are group of pixels having similar brightness values in the different spectral channels of data. The objective of classification is to match the spectral classes to the information classes of interest. In most cases there is not a simple one-to-one match between these two types of classes. Some information classes, like water, may contain a number of spectral subclasses with spectral variations. For example in the case of water, the spectral variation as explained before may be due to different turbidity, depth, floating vegetation or algae contents, etc or in the case of forest, the spectral variation may be due to variation in age, species and density. The final result of classification is a mosaic of pixels, each of which belongs to a particular category.

There are different classification methods. The two generic types of classifications are supervised and unsupervised classification. In a supervised classification, the analyst first identifies the imagery samples of different information classes (surface cover types) of interest. Then numerical information in all spectral bands for the pixels comprising these areas (classes) will be used as a reference data to "train" the image classifier or computer to recognize similar areas. The selection of right training areas is based on the analyst's visual skill, familiarity with the geographical area and his knowledge of the actual surface cover types depicted in the image. Thus the analyst is "supervising" the categorization of a set of specific classes. Because of the variety of reflectance pattern from water bodies, several training sets should be defined for different water classes based on visual differences in tone. Then the computer algorithm recognizes pixels of similar spectral reflectance and put them in the same class.

Unsupervised classification is reverse of the supervised classification process. Spectral classes are grouped first, based solely on the pixel brightness and numerical information in the data, and are then matched to different information classes. In this case usually, the analyst specifies how many groups or clusters should be looked for in the data. Some groups can be merged or break down later.

Classification can be done manually or by computer. In order to recognize reservoirs on a satellite image, the human mind makes use of several visual characteristics, such as shape, contiguity and the association with the drainage network (Liebe, 2002). In a different way, image processing software, such as ARCGIS and IDRISI, use the spectral information represented by digital numbers for recognition of water bodies.

3.5 Landsat images

Since in this paper Landsat images have been used for water surface delineation, Landsat specifications are briefly explained here.

The Landsat program has provided about 35 years of high spatial resolution data of the Earth's surface to a broad and varied user community. It is a major component of NASA's Earth observation program, which started in 1972 by Landsat 1. The mission of the Landsat program is to provide repetitive acquisition of high resolution multispectral data of the Earth's surface on a global basis (Landsat 7, Science Data Users Handbook,2006).
Launched in April 1999, Landsat 7 is currently the latest platform of the Landsat program. It is equipped with an "Enhanced Thematic Mapper Plus" (ETM+). ETM+ is a passive, optical across-track-scanner that measures solar radiation reflected or emitted by the Earth's surface. Table 4 shows the radio characteristics of Landsat 7 ETM+. ETM+ is the successor of the Thematic Mapper(TM) which was mounted on Landsat 4 and Landsat 5. Except the band 6 resolution which has been increased from 120 to 60 m, the other bands have the same resolution in both TM and ETM+. In the meantime a panchromatic eighth band with a resolution of 15 m was introduced to the ETM+ sensor for better accuracy.

Table 4: Landsat 7 ETM+ Radiometric Characteristics

(Source: Landsat 7, Science Data Users Handbook, 2006)

Spectral Resolution (µm)	Band	Spatial Resolution
Band 1: 0.450 – 0.515	Blue	30
Band 2: 0.525 – 0.605	Green	30
Band 3: 0.630 – 0.690	Red	30
Band 4: 0.760 – 0.900	Near IR	30
Band 5: 1.550 – 1.750	Mid IR	30
Band 6*: 10.40 – 12.5	Thermal	60
Band 7: 2.080 – 2.35	Mid IR	30
Band 8: 0.52 – 0.92	Pan	15

* Band 6 on Landsat 7 is divided into two bands, high and low gain.

The orbit of Landsat 7 is repetitive, circular, Sun-synchronous, and near polar at a nominal altitude of 705 km (438 miles) at the Equator. Circling the Earth at 7.5 km/sec, each orbit takes nearly 99 minutes. The spacecraft completes just over 14 orbits per day, covering the entire Earth between 81 degrees north and south latitude every 16 days (Landsat 7 science data user handbook, 2006).

Landsat 7 swath (field of view) size is approximately 185 km. The approximate dimension of a Landsat scene is 183 x 170 kilometers (GLCF Data Center) and they are indexed with path and row numbers according to the Worldwide Reference System (WRS).

3.6 Radar Altimetry

3.6.1 Overview

A Radar Altimeter (RA) is a nadir-pointing active microwave sensor designed to measure the surface elevation. Unlike other common instruments installed in satellites it is not an imaging device. The Radar Altimeter is a Ku-band (Operating at ~13.6 GHz) nadir device (i.e. it can observe the points directly below the satellite) which emits a series of microwave pulses towards the surface. By noting the two-way time delay between pulse emission and echo reception, the surface height can be determined. Radar Altimetry is not dependent on time of day and in compare to optical method and SAR is less dependent on weather and vegetation cover. It functions in two modes: ocean or ice and provides information on:

- Significant wave height
- Surface wind speed
- Sea surface elevation, related to ocean currents
- Surface geoid and tides
- Various parameter over sea ice and ice sheets

3.6.2 Altimeter missions

3.6.2.1 Previous missions

Radar Altimeter has been used for the first time onboard Skylab launched in 1973. It produced the first measurements of undulations in the marine geoid. A few years later GEOS-3 has launched in 1975 for Radar Altimetry purpose. It was the first satellite only dedicated to altimetry, but its low accuracy (about 2 m) made its data unusable to extract any scientific data. In 1978 NASA launched Seasat to study oceans. Seasat was the first satellite which reached a satisfying technological degree (noise level of the radar altimeter smaller than 10 cm). Later in 1985 US Navy launched GEOSAT. Table 5, shows a quick view of the history of major satellite altimeters.

Table 5 - Previous Radar Altimeter missions

Satellite	Operation	Repeat Period
Skylab	1973 -	-
GEOS-3	1975 -	-
SEASAT	1978	17 days
GEOSAT	1986-1989	17 days
ERS-1	1991-1996	35 days (phases C+G)
TOPEX/Poseidon	1992-2002	10 days

3.6.2.2 Current missions

Currently there are several Altimetry Satellite missions. Some of those are dedicated only for altimetry purposes (GFO & ICESat), while some do several tasks including Altimetry. Table 6, shows the current Radar Altimetry Satellite missions. Between these missions, ICESat track data wasn't accessible. Jason-1 has a very disperse track inland and can't be used for inland water measurements. Frappart et al 2006 mentioned that "Unfortunately, Jason-1 does

not provide land surface water measurements due to loss of surface lock by the onboard tracker and inaccurate retracking procedure over land surface water."

Table 6 - Current Radar Altimetry missions

Satellite	Launch date	Repeat cycle (day)	Orbit mean height (km)	Orbit period (min)	Space between track at Equator (km)
ERS-2	Apr. 1995	35	800	100	90
GFO	Feb. 1998 *	17	800	100	160
Jason 1	Dec. 2001	10	1335	-	315
Envisat	March 2002	35	800	100	90
ICESat	Jan. 2003	33	600	-	-

* The GFO satellite was launched in Feb. 1998, but due to some technical problem its operation was not accepted until Nov. 2000

3.6.2.3 Future missions

Future missions are required to provide better spatial and temporal coverage. Rosmorduc et al 2006 mentioned that for future RA missions consideration is now being given to altimetry missions capable of 'scanning' the ocean surface to acquire data at scales of a few tens of kilometers, passing over the same spots every few days. Other projects on the drawing board are based on constellations of dedicated, low-cost micro satellites.
According to Rosmorduc et al 2006, the following missions will be launched before 2010:

- Jason-2 (2008)
- Cryosat (2009)
- (Altika) (2009)

3.6.3 Principles

As a Radar Altimeter transverses over the Earth's surface, it continuously sends radar pulses and records the average surface `spot' heights. Each returned height value is an average of all surface heights found within the footprint of the altimeter. The footprint of a radar altimeter is the region on the sea surface (or ground surface) illuminated by the antenna beam angle. Later this article will show that the diameter of the footprint is between hundreds of meters to a few kilometers. Figure 10, illustrates the principle of satellite altimetry. According to the figure 10, the sea height can easily be computed by subtracting the corrected altimeter range from the orbital altitude:

$$H_{sea} = H_{orb} - h_{alt} \quad (1)$$

Horb= Satellite altitude above a reference ellipsoid;
halt= Measured and corrected altimeter height above the sea surface;
Hsea= Altimeteric sea surface height above the reference ellipsoid.

The accuracy of the absolute sea level measurements by a radar altimeter is therefore always limited by the accuracy of the computed satellite altitude. Higher accuracy can be obtained by Precise Orbit Determination (POD).

The sea surface height itself consists of the geoid height (permanent topography), sea surface (dynamic topography), tidal elevation (ocean tides, the polar tides related to the centrifugal force due to the Earth rotation) and inverse barometric effect (fittings of the water column's height in response to the atmospheric pressure variations).
While talking about heights, it is important to insist on the reference system, to avoid confusion. That is why we speak about "height relative to the ellipsoid (h)" or "height relative to the geoid (h-hg)" (Lellouch, 2006).

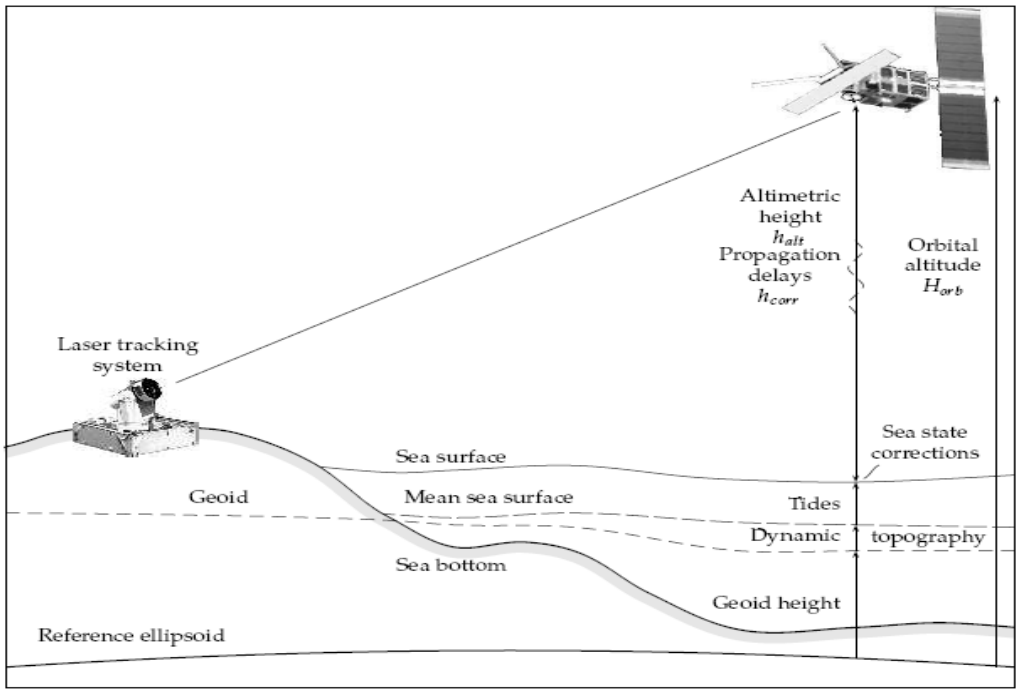

Figure 10, The principle of altimetry measurements (source: from Scharroo, 2002)

When a short pulse is propagating from the satellite to the sea surface, it expands spherically from a point to a disk, After the leading edge of the pulse strikes the sea surface, the area illuminated by the pulse becomes a circle that expands with time until the trailing edge of the pulse reaches the calm sea surface a time τ later, thereafter, the area illuminated by the short pulse becomes an expanding annulus (Chelton et al. 1989). Figure 11, illustrates the geometry of reflection of altimeter pulse from the surface. Consider a transmitted pulse with effective duration τ incident on a calm sea surface, Chelton et al 1989 showed that the area of the circular footprint contributing to the signal received by the altimeter at time τ and the area of annulus (between inner and outer boundary) contributing to the radar return is:

$$A_{\max} = \frac{\pi R_0 c \tau}{1 + R_0 / R_e} \qquad (2)$$

, where c is the speed of the light, Re is the radius of the earth, R0 is altitude of satellite above the nadir point. The denominator is a correction for the curvature of the earth's surface.

As Eq. 2, shows the maximum footprint area on a calm sea surface depends only on the effective pulse duration and the satellite altitude R0. Thus according to the formula, any desired footprint area can be achieved by adjusting the effective pulse duration appropriately (Chelton et al. 1989).

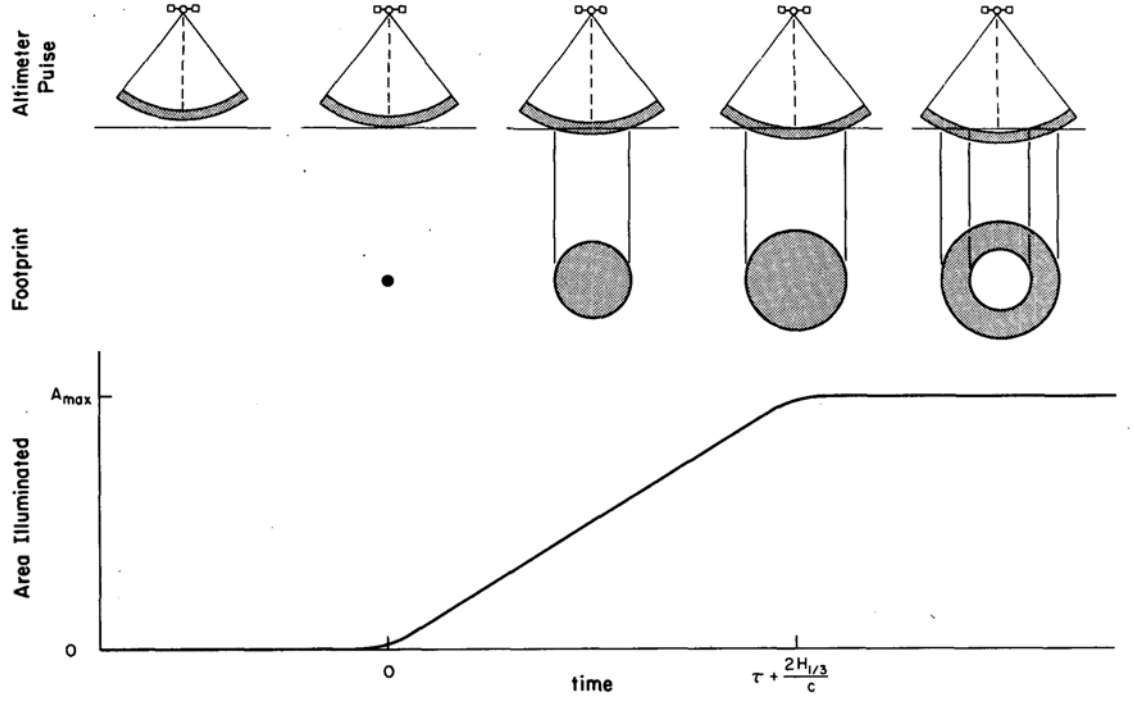

Figure 11- Short pulse propagating from the satellite and the footprint contributing to the radar return (Source: Chelton 1989)

The presence of waves increases the area on the sea surface contributing to the radar return. Chelton et al. 1989 shows that the maximum footprint area contributing to the radar return increases linearly with the Significant Wave Height (SWH), and can be calculated as:

$$A_{\max} = \frac{\pi R_0 (c\tau + 2H_{1/3})}{1 + R_0 / R_e} \qquad (3)$$

The effective pulse duration of the pulse from a Radar Altimeter is very short. The SEASAT, GEOSAT, and TOPEX altimeters all use effective pulse duration of 3.125 ns. Table 7, shows altimeter effective footprint diameter related to different Significant Wave Height (SWH).

For altimetric measurements of sea surface elevation, the antenna beam width should be large enough to filter out the effects of waves on the sea surface and to obtain a measure of mean sea level. Moreover, a broad beam width results in contamination of the measurement when land is present in the side lobes of the antenna pattern. A reasonable compromise is to design the altimeter so that the footprint diameter is a few km (Scharroo, 2002).

Table 7 - Altimeter effective footprint diameter as a function of Significant Wave Height (SWH) for satellites in altitudes of 800 km and 1335 km (Source: Chelton 1989)

Effective footprint diameter (km)		
Satellite Altitude (km) / SWH (m)	**800**	**1335**
0	1,6	2
1	2,9	3,6
3	4,4	5,5
5	5,6	6,9
10	7,7	9,6
15	9,4	11,7
20	10,8	13,4

The key principle behind the altimeter is that the information required is in the shape and timing of the returned radar pulse (ESA, 1992). The location of the point of maximum rate of increase (the leading edge), the slope of the increase and the total received power are three principle properties that are measured by a radar altimeter (Scharroo, 2002). This process is performed by an algorithm called tracker (Chelton et al. 1989). The information can be extracted from the waveform. An Altimeter waveform is the histogram of energy backscattered by the ground surface to the satellite with respect to time. Irregularities on the surface, larger than the pulse width, cause the returned pulse to be distorted and stretched (ESA, 1992). Therefore as figure 12 shows, an additional slope is imposed on the leading edge of the returned signal strength curve. This slope is related to the ocean wave height and the mid-point of this leading edge slope is equivalent to the reflection from the average position of the surface (ESA, 1992).

Acording to figure 12, the satellite-to-Mean Sea Surface (MSS) distance h can be calculated from the time delay τ between the transmitted pulse and the reception of the mid-point of the waveform's leading edge (Resti et al 1999). It should be noted that, the time delay between the transmitted pulse and the reception is quite a bit longer than the actual τ corresponding to the range. It is because, after arrival of the return pulse at the antenna dish, it follows a path to the altimeter instrument. This length and its corresponding time can be estimated or calibrated in a laboratory environment before launch. Assuming the radar pulse travels at the speed of light, C, the uncorrected altimeter range can be estimated by:

$$h_{alt} = \frac{C\tau}{2} \tag{4}$$

The Significant Wave Height (SWH) is related to the spreading of the waveform leading edge and can be calculated accordingly. Over the ocean surface, an empirical relationship can be used to convert the backscatter to an estimate of wind speed (Witter and Chelton, 1991).

Although their primary objectives are ocean and ice studies, altimeters are able to provide altimeter measurements of continental water heights. In particular, the ability to remotely detect water surface level changes in lakes and inland seas has been demonstrated (cited in GRM 2003 from Birkett 1994).

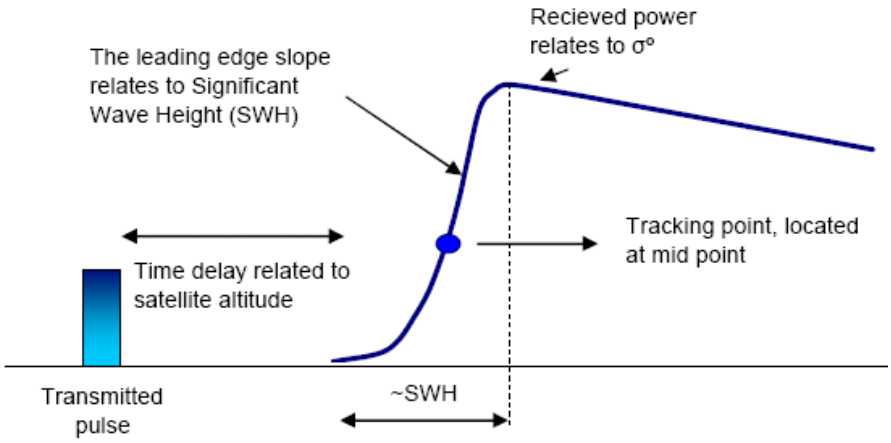

Figure 12 - The transmitted pulse, the shape of the echo from the ocean, and the parameters derived from it (Source: ESA 1992)

In reality, the surface backscattered signal is made up of different parts with different reflective coefficients, depending on their physical properties, and even they may have different heights. This will cause a noisy waveform having multiple peaks.

To have a good estimation of time delay, a full analysis of pulse shape should be done. Waveform retracking consists in a full analysis of pulse shape to obtain a better range estimate. During the retracking of waveform, the algorithm tries to fit the waveform to a special theoretical model. The special algorithm retrieves the point of the radar echo corresponding to the effective satellite to- ground range (Frappart et al 2006). After collecting meaningful radar echoes by the Radar Altimeter antenna, retracking extracts geophysical parameters as Geophysical Data Records (GDR).

In the past, Radar Altimeters did both collection of meaningful echoes and extracting of geophysical parameters onboard. But in recent altimeters (for example in Envisat) collection of meaningful radar echoes without any extraction of geophysical parameters is accomplished on-board; and the estimation of the relevant geophysical parameters is only implemented on the ground. This will provide more robust and autonomous instrument operation over different types of surfaces.

There are several retracking methods for different purposes and based on different theoretical models. The four major retracking methods are:

- Ocean retracker: It is intended for ocean surfaces and is based on a modification of Hayne's model
- Ice-1 retracker: It is intended for general continental ice sheets and is based on a model-free retracker called the Offset Centre of Gravity (OCOG) echo method
- Ice-2 retracker: It is optimized for ocean-like echoes from continental ice sheet interior, and is based on Brown (1977) model retracking algorithm
- Sea-ice: It is optimized for specular returns from sea-ice, it is a threshold retracking scheme for peaky waveforms developed by Laxon 1994

However, none of the above mentioned retrackers are intended for processing of the radar echoes over continental waters, but many references for example Frappart et al (2006), show that among the four major retracking algorithms applied to waveforms, Ice-1 provides the most suited ranges for continental hydrology and inland water studies.

Among the current RA missions, ENVISAT Geophysical Data Records products contain altimeter ranges derived from four retrackers (Frappart et al 2006). Unfortunately, Jason-1 does not provide land surface water measurements due to loss of surface lock by the onboard tracker and inaccurate retracking procedure over land surface water (Frappart et al 2006).

3.6.4 Sources of errors and required corrections

Many parameters affect the accuracy of altimeter data. The measurements contain noise, the computed orbit contains errors and the models are not perfect either. To obtain better accuracy, some geophysical corrections should be applied to the altimetry data. These corrections are usually available in the RA products.

As Eq. 1 shows, the accurate determination of the ocean height is dependent on determining the precise orbit height of the spacecraft above the center of the Earth. So it is important to determine the orbit of spacecraft precisely. This can be achieved by using different new technologies, but still some error may arise because of error in satellite orbit determination.

Refraction by neutral and charged particles in the atmosphere delays the radar pulse and lengthens the altimeter range (Scharroo, 2002). To compensate this delay, three types of corrections should be applied: dry tropospheric correction, wet tropospheric correction and ionospheric corrections.

Tidal elevation (solid-Earth tide & Ocean tides) is another source of error, caused by gravitational pull of the Sun and the Moon on the solid Earth and on the oceans.
Another source of error is because of interaction between radar pulse and ocean surface. Wave troughs reflect the pulse better than the wave crest, so the estimated range will be biased to the wave troughs. The sea state bias should be applied accordingly to correct this.
Table 8, shows the approximate contribution of main sources of errors in measurements, models and orbits in ERS and Topex satellite.

Table 8 - approximate contribution of errors in ERS and Topex (Source: Scharroo, 2002)

Source of Error	Error (Cm)	
	ERS	TOPEX
Altimeter range	3	2
Orbital altitude	5	2
Dry tropospheric correction	1	1
Wet tropospheric correction	1,5	1,5
Ionospheric correction	1	0,7
Ocean tides	3	3
Solid Earth tides	0,5	0,5
Inverse barometer correction	2	2
Sea state bias	1	1
Sea surface variability	4	4
Mean sea surface	11	11

As the figure 13 shows, RA missions achieved higher accuracy by development of new techniques, but still more effort is required.

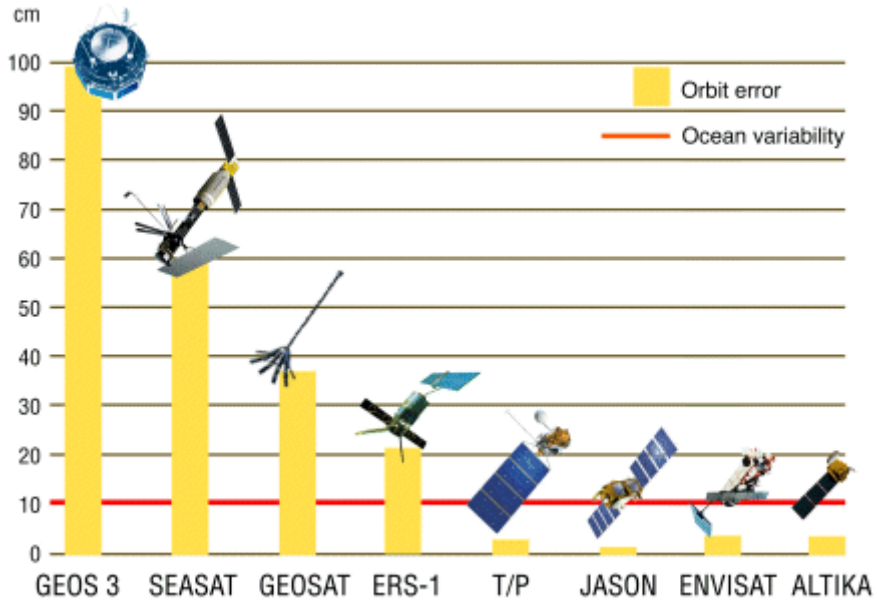

Figure 13 - Improvements in measurement accuracy of satellite altimetry

(Source: Rosmorduc et al 2006 - Credits CNES)

3.6.5 Advantages and Limitations of Radar Altimetry

RA has the following advantages:

- Radar Altimetry has the advantage of being able to take global, homogeneous, repeated measurements thus enabling systematic monitoring to be carried out over several years
- RA is independent of light. It can be used in day/night and all weather operation
- In comparison with the optical method and SAR, It is less affected by vegetation or canopy cover
- Potential to estimate the height information for any target beneath the satellite overpass
- Ability to monitor seasonal and annual variations,

RA has the following limitations:

- The satellites repeat-orbits are rather long (10 to 35 days), which do not suit for real-time monitoring of water levels is rivers or lakes, but is suitable for seasonal or interannual monitoring of water level.
- These instruments are primarily designed to operate over uniform surfaces such as oceans and ice-sheets. Highly undulating or complex topography may cause data loss or non-interpretation of data (Frappart et al 2006). This makes it difficult to use RA for inland water monitoring.
- Retrieved heights are an "average" of all topography within the instrument footprint. The basic distributed data (GDR) are mainly average over one second, thus covering about 7 km on the ground (data averaged over 1/20 s do exist, however). For example the ERS altimeters transmit 1020 pulses per second. Since the return from one pulse produce a waveform that is too noisy to accurately pinpoint the leading edge, 50 pulses are averaged into one waveform. Hence measurements are produced at a rate of roughly 20 Hz. The precision of the measurements is again boosted by averaging 20 elementary measurements into one 1-Hz measurement (Scharroo, 2002).

- The height accuracy is dominated by knowledge of the satellite orbit, the altimetric range (distance between antenna and target), the geophysical range corrections and the size and type of the target.
- Unlike imaging instruments, altimeters only retrieve heights along a narrow swath determined by the instrument's footprint size. This will limit the chance of use of satellite altimetry information for different targets.
- Minimum target size is controlled by the instrument footprint size and the telemetry/data rates, and also on the surrounding topography and the target-tracking method used.
- The satellite orbit scenario and target size also determine the spatial and temporal coverage. Improved temporal coverage is gained at the expense of spatial coverage for a single satellite mission.
- Major weather changes including wind events, heavy precipitation, tidal effects and the presence of ice may affect data quality and accuracy.
- In reality the time intervals of sampling of RA over lakes and rivers are quite often greater than their theoretical values, due to gaps in measurement series caused by limitations of the waveform retracking algorithms (for instance, over the Amazon basin Topex Poseidon shows a 40 to 50 days effective sampling period at low river stage).
- One other important problem in repeated track is that the tracks are not truly repeated and may be located a couple of kilometer from each other. So in some cases it is not really possible to have data from a small lake or river
- The number of points within a virtual station is proportional to the area of the satellite trace-water intersection. Consequently, small virtual stations require high quality measurements.

4 Results

4.1 Optical method and SAR

4.1.1 Available satellites and time schedule of image acquisition

A list of the main earth observation satellites in the optical range and radar, has been attached in appendix 1 and 2. For this case study based on the size of the region and reservoirs, those satellites with a resolution of about 20 – 50 m have been selected as the proper satellites suitable for the project. Optical satellites and radar satellites have been listed in table 9, and 10 consequently.

Table 9 - Earth observation satellites (optical) suitable for this project

No.	Satellite System	Year of launch	Country	Resolution in meters & Nr. of bands			Revisit/Pointing **
				Pan *	Ms *	Tir *	
1	ALOS	2006	Japan	2.5	10 (4)		46 days/yes (ms)
2	ALSAT-1 (DMC)	2002	Algeria		32(3)		
3	BEIJING-1 (DMC)	2005	China	4	32 (3)		
4	BILSAT (DMC)	2003	Turkey	12	26 (4)		
5	CBERS 1+2	1999+2003	China+Brazil		20(4),80(3),260(2)	80 (1)	26 days
6	DMC Surrey (5x)	2006-	UK		32 (3)		
7	EO 1	2000	USA	10	30(10),30(220)		
8	IRS 1C/D	1995-1997	India	5.8	23.5 (4)		24 days/yes (pan)
9	IRS P2	1994	India		36 (4)		24 days
10	IRS P6 (Resourcesat 1)	2003	India		5.8(3)/23.5(4)/56(4)		5 days/24 days
11	Landsat 4	1982	USA		30 (6)	120 (1)	16 days
12	Landsat 5	1984	USA		30 (6)	120 (1)	16 days
13	Landsat 7	1999	USA	15	30 (6)	60 (2)	16 days
14	MTI	2000	USA		5(4), 20(9)	20(3)	
15	NigeriaSat-1 (DMC)	2003	Nigeria		32 (3)		
16	PROBA (CHRIS)	2001	Europe	5	18 (18)		7 days
17	RESURS-01-3	1994	Russia		34(3) / 137(4)	548 (1)	18 /5 days
18	RESURS-01-4	1998	Russia		34(3) / 210(4)	700 (1)	18 /5 days
19	SAC-C	2000	Argentina	35	175 (5)		9 days
20	SPOT 2	1990	France	10	20 (3)		4 days
21	SPOT 4	1998	France	10 (band2)	20 (3) / 1000 (4)		4 days / 1 day
22	SPOT 5	2002	France	5(2.5) / 10	10(3)/20(1)/1000 (4)		5 / 26 / 1 days
23	Terra ASTER	1999	USA		15(3) /30(6)	90 (5)	16 days
24	UK-DMC (DMC)	2003	UK		32 (3)		

* (Pan: Panchromatic – Ms: Multi Spectral - TIR: Thermal InfRared)

** Pointing: Refers to the capability to focus the sensor in any direction away from the satellite path

Table 10 - SAR satellites suitable for the case study

No.	Satellite System	Year of launch	Country	SAR Resolution (m)	Swath (km)	Orbit height	Revisit
1	ALOS	2006	Japan	10/20/100 (L-band)	35/70 | 70/250	700	46 days
2	Envisat ASAR	2002-03	Europe	30 (C-band)	60-100	800	35 days
3	ERS 2	1995	Europe	25 (C-band)	100	780	35 days
4	IRS P4 (Oceansat)	1999	India	7, 11, 18, 21 GHz	1420	720	2 days
5	QuikSCAT	1999	USA	13.4 GHz	1800	803	
6	Radarsat 1	1995	Canada	8-100 (Cband)	50-500	798	24 days

4.1.2 Time schedule for satellites passing the region

To have a more realistic answer to the question of feasibility of the use of optical methods and SAR imagery, a preliminary time schedule of available satellites and their overpass time should be created. To create such a time schedule, two main approaches can be used. The first approach is to use satellite simulation (Tracker) software, which virtually simulates satellite orbits and shows their locations in a specific time. There is different satellite tracker software available. For example European Space Agency (ESA), provides an online Java version of satellite tracker by the name "Earth View". It is a user friendly program which can be accessed at: (http://www.eoportal.org/orbits/view_envisat.html). Using these software, it is possible to approximately find when a satellite is passing the region of interest.

The second and more accurate approach is based on the time series of previous acquired satellite images of the region. Different image catalogues/portals can be used to browse available scenes from the region observed by different satellites. By checking Meta data of the scenes, acquisition date and footprint of the scenes can be found. Then acquisition date of each scene should be converted to a number based on its year, month and day of acquisition. These numbers will repeat periodically based on their relevant satellite period. Based on these time series and according to the satellite period, the time series can be extended for future acquisition. The time series can then be entered to one scheduling program like Microsoft Project (MSP). Here because of a limitation in MSP (recurrence interval of recurring tasks can not exceed 12 days in MSP version 2003), calendar option in Microsoft Outlook and Microsoft Excel have been used instead.

In this part, time schedule for 3 main satellites carrying optical sensors (Landsat, ASTER, SPOT) and 2 satellites carrying SAR (Envisat , ERS2) have been produced based on the abovementioned method. Table 11 depicts these satellites and their relevant sources of data. It should be noted that among these satellites two pairs have similar orbit with a small time lag. ASTER has the same orbit as Landsat 7, but is 30 minutes behind Landsat. Similarly Envisat flies the same orbit as ERS-2, with the only difference of having 30 min. time lag. Members of each pair acquire the images of a region in the same day. Accordingly, However totally 5 satellites have been considered in this part, but actually they act like 3 independent satellites.

Table 11- Satellites considered in the time schedule for table 14

No.	*Satellite name*	*Catalogue service*	*Period (day)*
1	Landsat	USGS Global Visualization Viewer (EROS)	16
1'	ASTER	USGS Global Visualization Viewer (EROS)	16
2	ERS-2	EOLI-SA	35
2'	Envisat	EOLI-SA	35
3	Spot	EOLI-SA	26

Figure 14, shows that three Landsat images (Pass/Row: 168/77,168/78 & 169/78) cover the whole Incomati basin and table 12 summarizes the reservoirs observed in each Landsat scene.

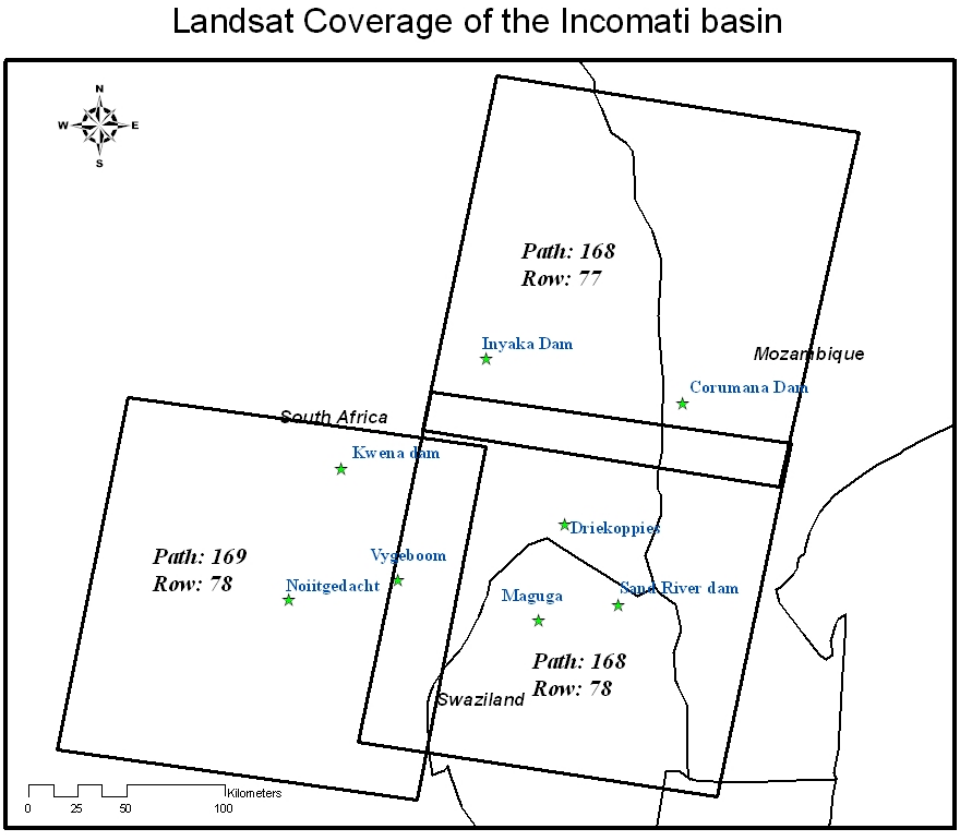

Figure 14 - Three Landsat images (Path/Row: 168/77,168/78,169/78) cover the main reservoirs in the Incomati basin

Table 12 - Landsat coverage of the main reservoirs in the Incomati basin

Path	*Row*	*Reservoir*
168	77	Inyaka Dam, Corumana Dam
168	78	Vygeboom dam, Driekoppies dam, Maguga dam, Sand river dam
169	78	Vygeboom dam, Kwena dam, Nooitgedacht dam

Eight ERS-2 /Envisat tracks observe the Incomati basin. These tracks are summarized in table 13 and coverage of the region by ERS 2 has been attached in appendix 3.

To illustrate more, April of 2007 has been selected randomly and the satellites' overpass time has been depicted in table 14. As table 14 shows these satellites completely cover the region during the month with an average of about 6 scenes per each reservoir per month. This gives a good flexibility. If in some cases an image can not be acquired from one satellite, other satellites can be used.

Table 13 – ERS-2 / Envisat coverage of the main reservoirs in the Incomati basin

Track No.	***Ascending / Descending***	***Repeated days in a 35 day cycle***	***Observed reservoirs***
49	D	13	Maguga, Driekoppies, Injaka, Sand River dam
85	A	16	Maguga, Driekoppies, Injaka, Sand River dam
92	D	16	Kwena, Nooitgedacht
128	A	19	Nooitgedacht
278	D	29	Corumana, Sand River dam
314	A	32	Corumana, Sand River dam
321	D	32	Kwena, Injaka, Vygeboom
357	A	35	Kwena, Vygeboom

Table 14 - Image acquisition time schedule for the reservoirs in the Incomati basin during April 2007

Reservoir / Day	Corumana	Maguga	Driekoppies	Kwena	Injaka	Vygeboom	Nooitgedacht	Sand River
1								
2								
3								
4				L		L	L	
5		E	E		E			E
6			S					S
7								
8		E	E	E	E		E	E
9								
10								
11						S	E / S	
12								
13	L	L	L		L	L		L
14								
15								
16	S							
17								
18								
19								
20				L		L	L	
21	E	S			S			E
22								
23								
24	E			E	E	E		E
25								
26				S				
27				E		E		
28								
29	L	L	L		L	L		L
30								
Total No. of shots	5	5	5	6	6	7	5	7

(E: Envisat / ERS - L: Landsat / ASTER - S: Spot)

4.1.3 Cloud Coverage (CC)

As explained before in part 3.2.3, while using optical methods, clouds are one of the main obstacles and a probability analysis should be done. For analysis of cloud cover probability in the region, meta-data from Landsat scenes archive at USGS has been used. Meta data includes key information like row No., path No., date and time of acquisition, sun azimuth, sun-elevation, cloud coverage and other useful information. Statistics were constructed from 204 scenes of the region, collected between 1985 and 2003. Table 15 summarizes the statistics of the scenes in different months. As explained before in part 1.2 the basin lies entirely within the summer rainfall region (October–March). During these months, in some cases, cloud coverage of up to 99% may make optical remote sensing of ground features impossible.

As figure 15 shows in most period of the year it is probable to obtain a scene with less than 50% Cloud Coverage (CC). From December to March the chance of acquiring a scene with CC of less than 50% is less in comparison to other periods of the year, however still it is more than 50% chance to obtain such a scene. During September, the chance of acquiring a scene with CC of less than 50% is below 50% and it is more probable that cloud obstacles the view of some reservoirs.

Although somewhat arbitrarily selected, this threshold of 50% likely represents the mean allowable value for water body detection.
Some references suggested different threshold. For example Asner 2001, cited from Yanesse et al. 1997 that it is difficult to assess land-cover change in a region when cloud cover is consistently 30% or more. At higher cloud cover values, cloud shadows become increasingly problematic and consistent spatial coverage of 'clean' pixels diminishes (Asner 2001).

Table 15 - Summary of cloud coverage (CC) information in the Incomati basin, based on 204 scenes obtained between 1985 and 2003

Month	Max CC (%)	Ave. CC (%)	No of scenes with CC < 50%	Total No. of scenes	Probabilities of obtaining a scene with less than 50% cloud coverage (%)
Jan	80	42	13	23	57
Feb	96	45	12	22	55
Mar	82	39	13	22	59
Apr	70	11	6	7	86
May	87	23	8	10	80
Jun	40	7.5	10	10	100
Jul	40	8	9	9	100
Aug	74	13	18	20	90
Sep	95	40	8	17	47
Oct	99	37	18	27	67
Nov	90	34	9	14	64
Dec	93	40	13	23	57

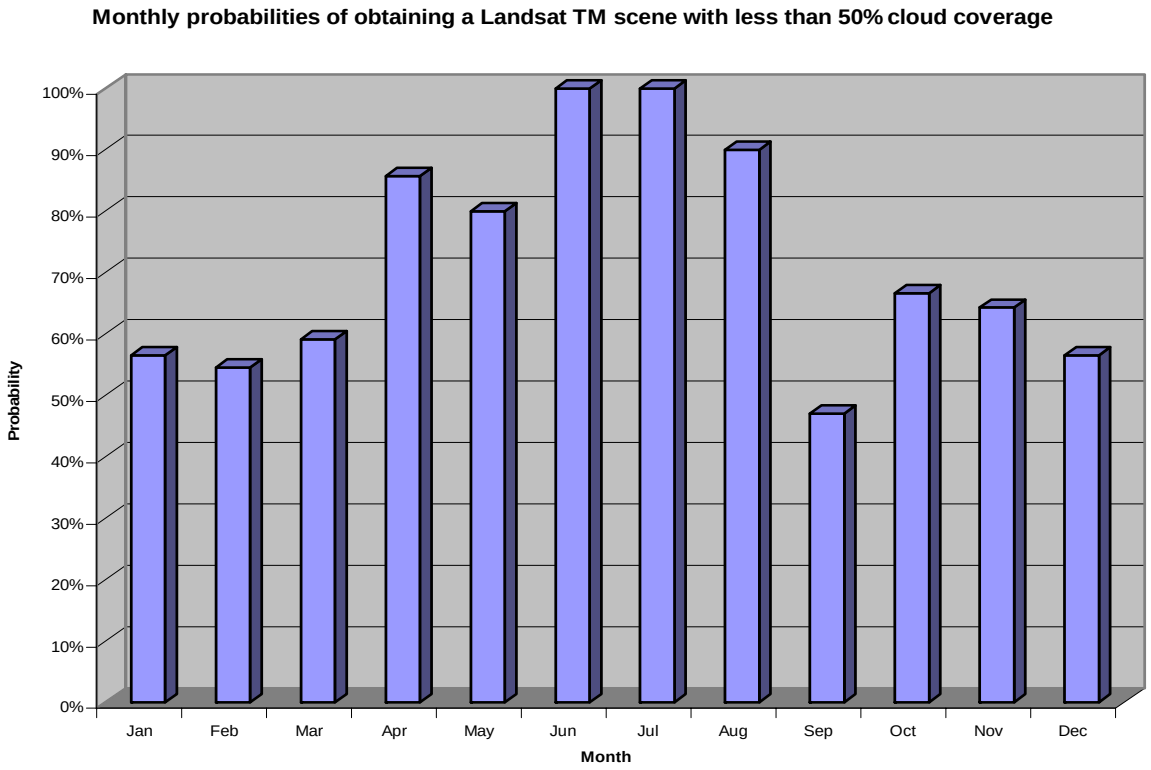

Figure 15 - Monthly probabilities of obtaining a Landsat scene with less than 50% cloud coverage from the Incomati basin

4.1.4 Water surface area estimation by optical method

In this part, Landsat images have been used as the major data for water surface delineation. However most of the images must be purchased from the provider(s), but some are freely available. Free Landsat images of the region have been downloaded using Earth Science Data Interface (ESDI) at the Global Land Cover Facility (GLCF) (www.landcover.org). Six cloud free images were available for this case study which has been summarized in table 16. According to the method and instruction, Landsat TM ETM+, image band 4 has been used for surface water delineation. Scenes parameters have been depicted in Appendix 4.

Table 16 - Landsat TM, & ETM+ images used for water surface delineation

No.	Pass/Row	Acq. date	Sensor	Attribute	Type	Location
1	168/077	6/25/1990	TM	Ortho, GeoCover	GeoTIFF	Mozambique, South Africa
2	168/077	5/30/2001	ETM+	Ortho, GeoCover	GeoTIFF	Mozambique, South Africa
3	168/078	6/25/1990	TM	Ortho, GeoCover	GeoTIFF	Mozambique, South Africa, Swaziland
4	168/078	5/30/2001	ETM+	Ortho, GeoCover	GeoTIFF	Mozambique, South Africa, Swaziland
5	169/078	3/9/1989	TM	Ortho, GeoCover	GeoTIFF	South Africa, Swaziland
6	169/078	5/21/2001	ETM+	Ortho, GeoCover	GeoTIFF	South Africa, Swaziland

(Landsat images have been obtained from the Global Land Cover Facility (GLCF), www.landcover.org.)

In each reservoir, there is a relation between water level and water surface as well as between water level and water volume of the reservoir. This relation depends on the topography of the reservoir. The Water surface can be calculated by measuring area between different contour levels and the water level-water surface curve can be calculated accordingly. The total water volume is the summation of water volume between different contour levels down to the lowest contour at the bottom of the reservoir. The water storage volume- water level relation can be calculated by integration of the water surface – water level relation. Water level-surface-storage data has been obtained from Department of Water Affairs and Forestry - South Africa (DWAF). These Water level-surface-volume curves have been attached in the appendix 5.

Since there are only a few reservoirs in this project, to minimize the classification error, manual classification has been used to delineate the water surface of the reservoirs in the available Landsat images. This is a little bit time consuming, but provides better and more accurate representation of water bodies in the region. Figure 16 shows the result of water surface delineation for Kwena Dam.

Ground truth information of water level has been obtained from Department of Water Affairs and Forestry - South Africa (DWAF).

For water assessment of a reservoir, first the reservoir's water surface has been delineated using ArcGIS software and water surface area has been calculated. Then based on the water level- water surface – water storage curve of the reservoir, in appendix 5, the relevant water storage volume has been estimated. Ground truth information has been used to have the actual water level of the reservoir on the acquisition date of image and to estimate actual water surface/water storage based on available curves in appendix 5.

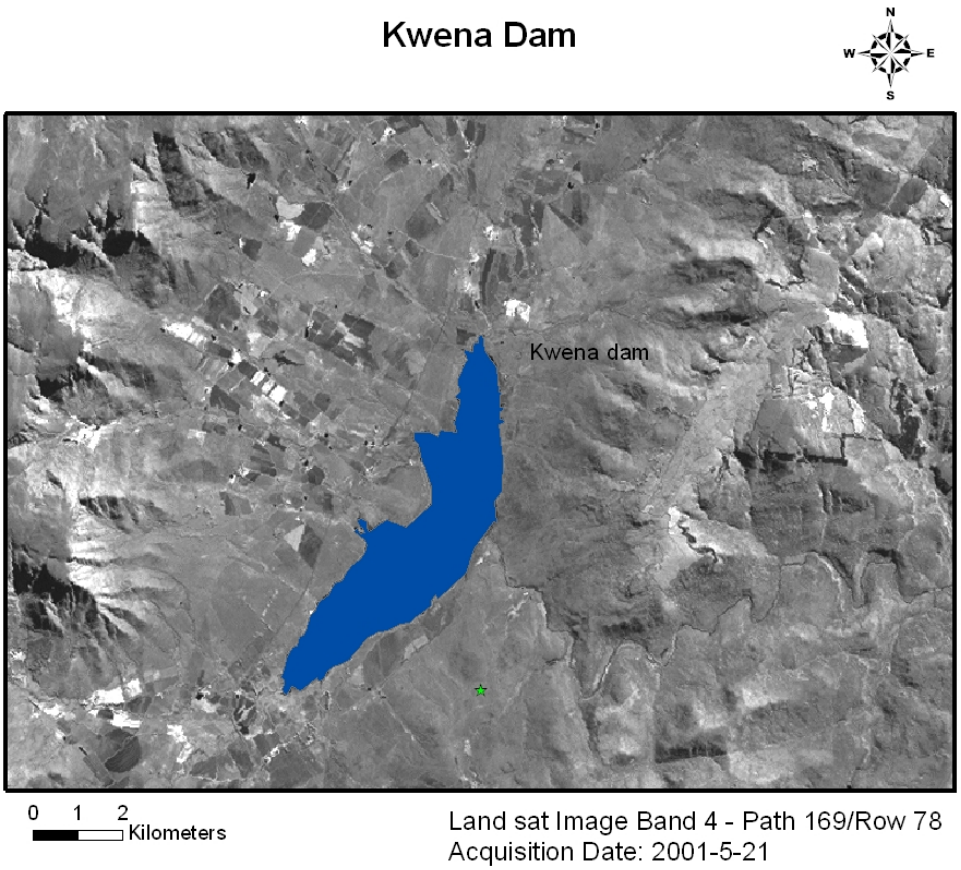

Figure 16 - Water surface delineation with Landsat Band 4 – Kwena dam

Table 17, shows the results of water surface delineation and comparison with the ground truth information. As table 17 shows, the maximum error is 7.5% in estimation of water surface and 8.5% in estimation of water storage. Generally error in the volume estimation is higher than that of surface estimation, because as explained before, water level-water volume relation is in higher degree than water level – water surface relation and it generally increases the error. It should be noted that ground truth information of the Corumana dam have been obtained from another source which may be a source of discrepancy between results.

Required accuracy:
Among many factors, the required accuracy depends mostly on the geopolitical condition of the region. When there are some arguments more accuracy is required and in normal time some lower accuracy can be acceptable.

Table 17 - Result of water surface delineation from Landsat TM and ETM+ Band 4, for the reservoirs in the Incomati basin

No.	Reservoir name	Image Acquisition Date	Estimated parameter (RS)		Ground truth information (GR)			Error	
			Water Surface (ha)	Water Storage (Mm^3)	Water Level (m)	Water Surface (ha)	Water Volume (Mm^3)	Surface Error $(A_{RS}-A_{GR})/A_{GR}$%	Volume Error $(V_{RS}-V_{GR})/V_{GR}$%
1	Kwena dam	2001/5/21	1266	162.1	36.54	1254	159.5	1.0%	1.6%
2	Vygeboom dam	2001/5/21	669	83.2	20.76	670	83.5	-0.2%	-0.4%
3	Nooitgedacht dam	2001/5/21	668	63	25.13	640	59.1	4.4%	6.6%
4	Driekoppies dam	2001/5/30	1849	246	28.58	1875	252.5	-1.4%	-2.6%
5	Corumana dam	1990/6/25	3477	349.5	102.17	3760	381.8	-7.5%	- 8.5%
6	Kwena dam	1989/3/9	1284	165.2	36.6	1257	160.1	2.2%	3.2%
7	Vygeboom dam	1989/3/9	673	84.2	20.87	675	84.3	-0.3%	-0.1%
8	Nooitgedacht dam	1989/3/9	674	64.1	25.55	659	62	2.3%	3.4%

Accuracy of the result depends on:

1- Weather condition
2- Moisture of surrounding areas as discussed before
3- Topography: another important factor affecting the accuracy of result is topography. In reservoirs with very steep sides, higher water surface accuracy is required because storage – surface curve is very sensitive to a small change in water surface. But in shallow lakes, storage – surface curve is less sensitive and lower accuracy can be acceptable
4- Ratio between area and perimeter of water

4.2 Radar Altimetry (RA)

4.2.1 Overview

In this part the feasibility of using the Radar Altimetry (RA) method for the case study has been checked. Based on the information in table 12, three Landsat images covering the Incomati basin have been merged together to have an overall satellite image of the region. The major reservoirs have been located over the overall image. Maguga Dam was commissioned in 2002, after the date of the last available free Landsat image of the region, so it can not be precisely located over the map and was approximately shown by a point and was excluded from the project.

A Mapping/GIS software should be used to overlay different RA tracks (defined by their location, latitude/longitude) over the satellite image of the region. The intersection between the reservoir and the satellite ground-track, if any, defines a so-called virtual station. Every point within the virtual station provides a virtual measurement of water surface. Since the altimeter beam has a certain width, sometimes, footprint may contain information obtained from dry land beside the reservoir.

Satellite orbit data and ground track information have been collected from RADS (http://rads.tudelft.nl/). The Radar Altimeter Database System (RADS) is an effort in establishing a harmonized, validated and cross-calibrated sea level data base from satellite altimeter data. RADS is run by the Department of Earth Observation and Space Systems of the Faculty of Aerospace Engineering, Delft University of Technology, the Netherlands. The RADS data base aims at users at both expert level like geoscientists and entry level, like advisory councils, water management authorities, teachers, and students. The purpose of RADS is for open sea water, but of course ground track information of the RA satellites are the same for both open sea and inland water.
The reason for choosing RADS for this part of the project was the simple ASCII file structure output of RADS, which needs less time for organizing and interpreting data.
After downloading RADS data, it has been filtered and formatted in another way using MATLAB, and then a database of different passes of different RA satellites has been created in Microsoft Access. This database can easily be used for any feasibility study of other RA projects and can be very useful for further similar projects.
ArcGIS then has been used to integrate the database of RA tracks with the satellite image of the region and to overlay it over the image of the region.

Among the current RA missions, as explained before, the feasibility of three missions will be checked.

4.2.2 GFO Satellite

Figure 17 shows the footprint of GFO satellite in the region. As the figure shows GFO passes Nos. 12, 143, 229, 414 cover the region. Among the main reservoirs only one (Vygeboom) is located very close to the footprint of GFO pass No. 414.
GFO tracks within some regions including South Africa are very disperse and many points are missing. So when plotting the actual footprint points it is realized that it is not feasible to use GFO because there is no real point of satellite orbit in the reservoir.

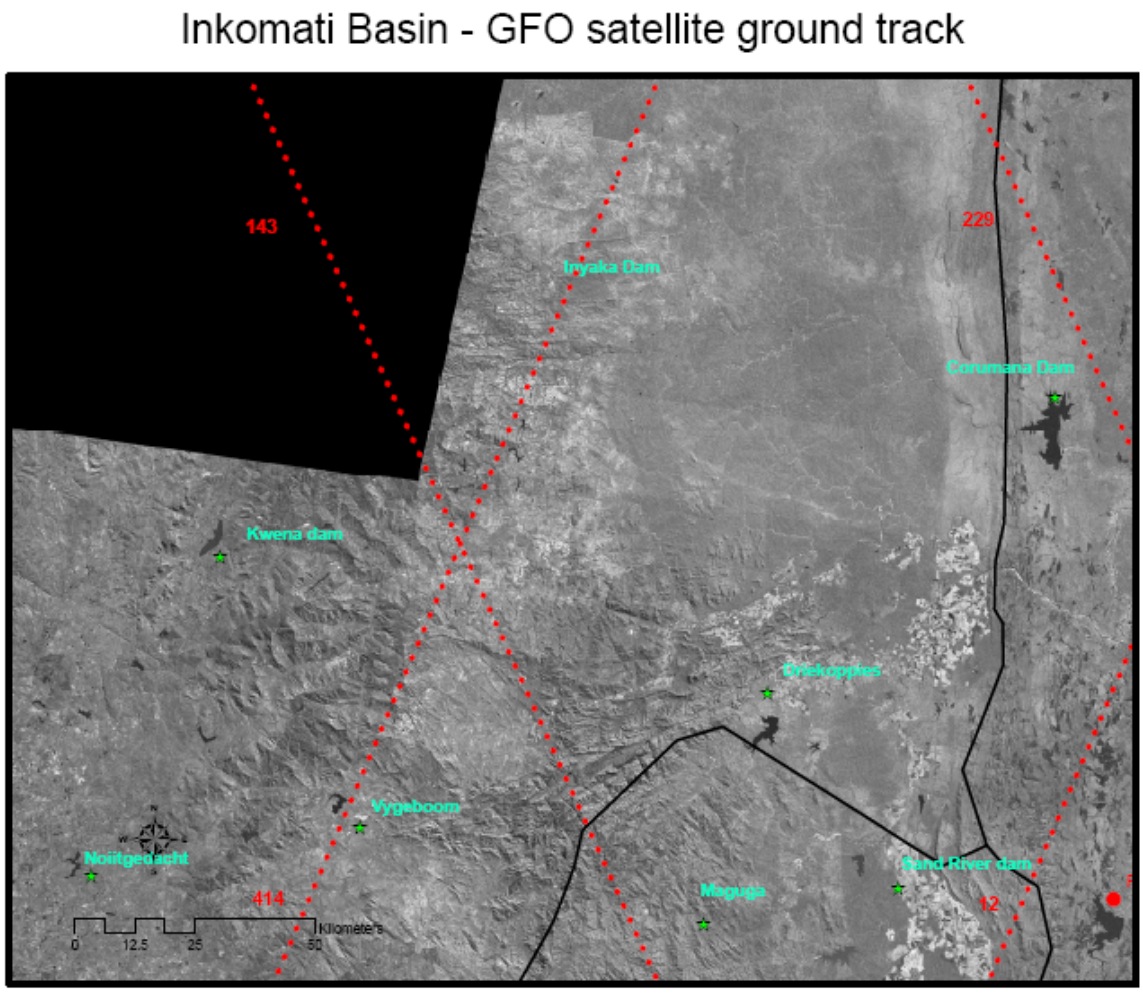

Figure 17 - Incomati Basin - GFO satellites ground track (This figure is best viewed in color)

4.2.3 Envisat / ERS2 Satellite

Figure 18 shows the footprint of Envisat & ERS2 satellite in the region. (Envisat and ERS-2 have the same orbit but with different passing time) As the figure shows Envisat passes Nos. 270, 356, 457, 543, 728, 814, 1001 cover the region.

Among the main reservoirs of the region, only "Noiitgedacht" is probably within the footprint of the Envisat satellite pass No. 356. Later this reservoir has been zoomed in, to see more detail condition of the track 356 and the reservoir.

Figure 19, shows a more zoomed image of the Noiitgedacht dam with the location of virtual stations from pass No. 356 of Envisat. As the figure shows about 50% of the virtual stations shown here are completely outside the reservoir. This is because as explained before in part 3.6.5.2 the satellite does not exactly follow the same orbit in different cycles and the orbits can be a few kilometers from each other in different cycles.

Among the nadir points located within the reservoir, still it should be checked whether those points will provide enough useful data for water level estimation or not.
Referring to table 7, since Envisat is orbiting at 800 km, assuming the water surface is smooth and there are some minor waves we find the effective diameter of footprint of Envisat as 1.6 km while average width and length of the Noiidgedacht dam are about 600 m and 7300 m.

Therefore most of the footprint's reflections are from surrounding areas not from the water surface. This will make it almost impossible to obtain useful data from these virtual stations.

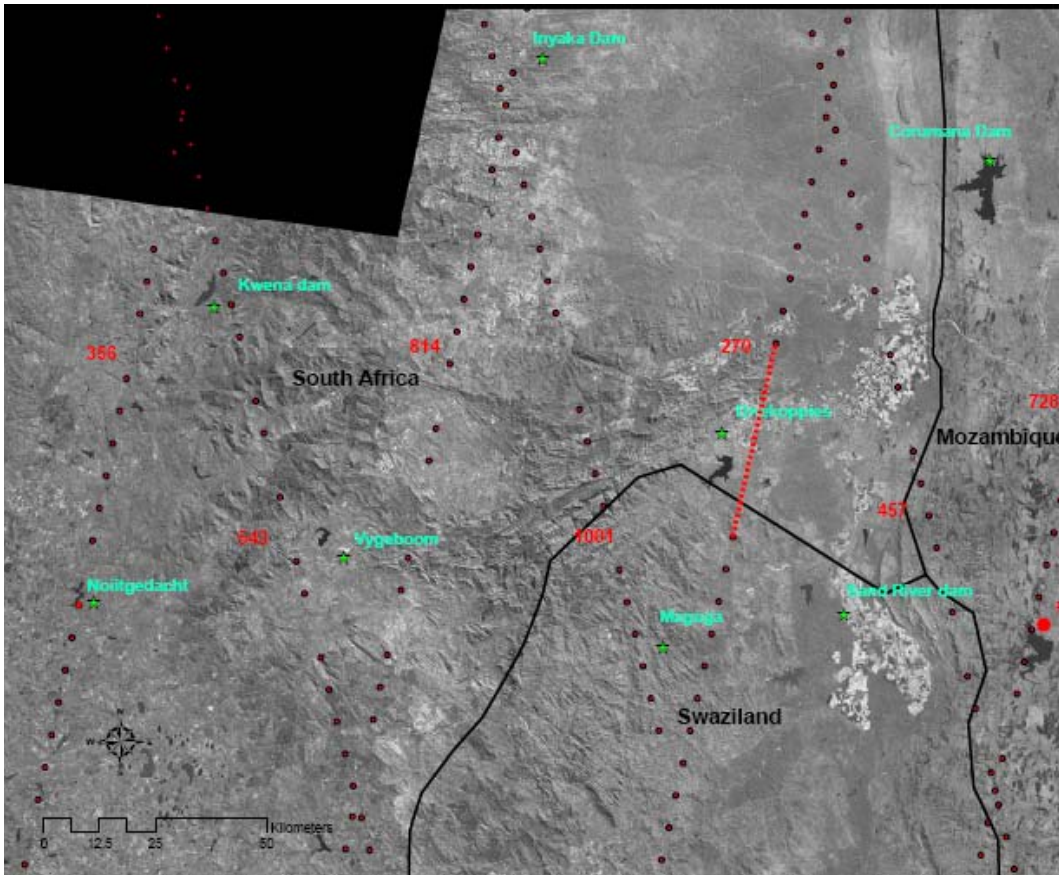

Figure 18 - Incomati Basin - ENVISAT & ERS2 satellites ground track

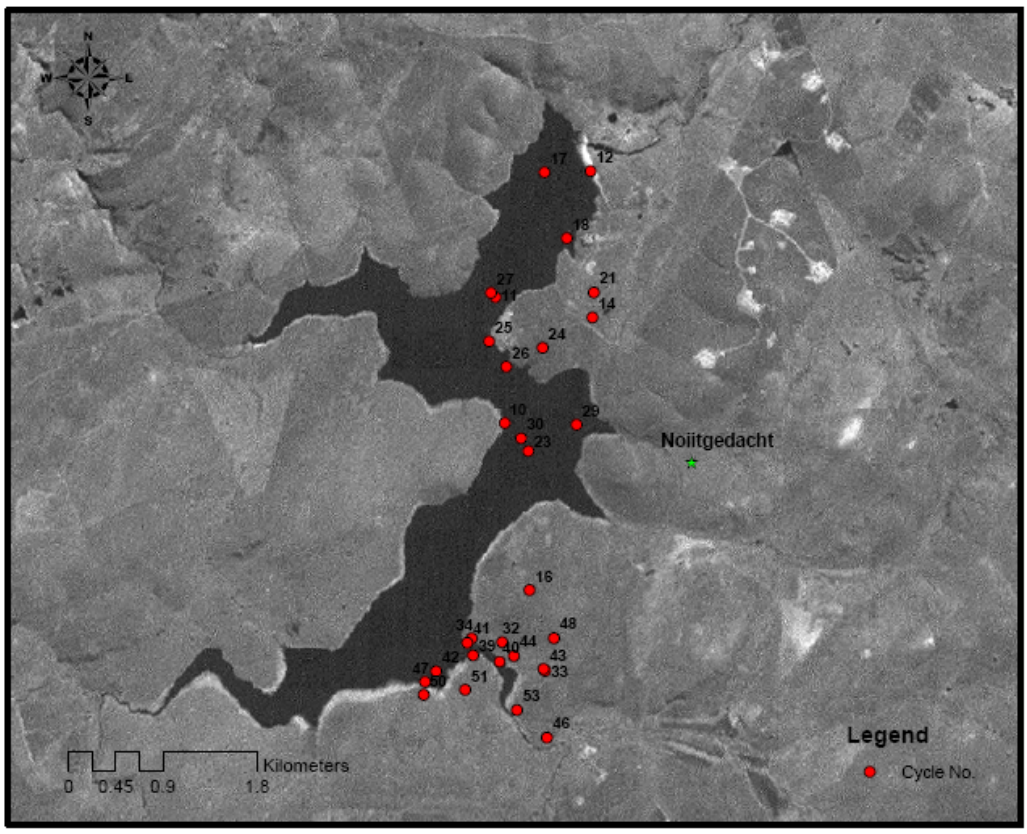

Figure 19 – Envisat pass No. 356 hitting Noiitgedacht Dam

5 Conclusion

As this study shows, among the three main Remote Sensing methods, two of them (Optical methods & SAR) can be used as suitable tools for monitoring of water resources in the Incomati basin. This will help the three countries sharing the basin to have a common estimation about the water storage. Based on the reservoir size and location, the third method, RA, can not be used for evaluation of water resources in this project. Although very useful in principle, RA has some limitations dealing with inland waters especially when the reservoirs sizes are not large enough.

Based on the literature review in the optical method, visible and near-infrared bands (wavelength 0.7 - 3.0 μm) are the most suitable bands for water surface and water storage estimation. These bands align itself with Landsat TM band 4 and SPOT-HRV band 3. In the SAR methods, high incidence angles (greater than 45 degrees) and HH polarization will give a suitable result.

Results obtained from 6 Landsat TM and ETM+ images showed high accuracy of water storage estimation with an average accuracy of 3.5%. After interpreting remote sensing data and water storage estimation, sources of errors like spectral overlap, very moist or waterlogged soil surrounding the reservoir and floating vegetation should be taken into account. Further RS data is required to propose a correction for the above sources of errors.

The image acquisition time schedule for the region shows high temporal resolution. In a month, different satellites acquire scenes from the region which gives good flexibility. A constellation of three independent satellites provides an average of 6 scenes per each reservoir per month. If one satellite can not obtain a suitable scene from a reservoir, because of technical problems or other hurdles (like high cloud coverage), the scene can be obtained from other satellites.

In some periods of the year, especially during the rain season, high cloud coverage of up to 99% may prevent acquiring a cloud free scene and will prevent the use of optical methods. In this case, SAR can be used instead, because of its advantage of functioning in nearly all-weather conditions. Alternatively, scenes obtained from other optical satellites during the next days can also be used.

6 References

1- A. Resti, J. Benveniste, M. Roca , G. Levrini , J. Johannessen , 1999 , *The Envisat Radar Altimeter System (RA-2)*

2- Birkett, C.M., 1998, *Contribution of the TOPEX NASA radar altimeter to the global monitoring of large rivers and wetlands*. Water Resour. Res., 34 (5), 1223-1239, 1998.

3- Brian Alan Riordan, 2005, *Using remote sensing to examine changes of closed basin surface water area in interior Alaska*

4- Carmo Vaz, A. & P. van der Zaag, 2003. *Sharing the Incomati waters: cooperation and competition in the balance*, UNESCO - IHP Technical Document / PCCP series number 13. UNESCO, Paris.

5- David G. Barber, Klaus P. Hochheim, Roy Dixon, David R. Mosscrop, Michael J. Mcmullan, 1996, *The role of Earth Observation Technologies in Flood Mapping: A Manitoba Case Study*, Canadian Journal of Remote Sensing, 22,1,137-143

6- Dudley B. Chelton, Edward J. Walsh and John L. Macarthur, 1989, *Pulse compression and sea level tracking in satellite altimetry*, J. Atmos. Oceanic Technol. , Vol 6 , 407 – 438

7- *ESA Technical Series (SP-1146)*, 1992, *ERS-1 system*

8- Fre´de´ric Frappart, Ste´phane Calmant, Mathilde Cauhope´, Fre´de´rique Seyler, Anny Cazenave, 2006, *Preliminary results of ENVISAT RA-2-derived water levels validation over the Amazon basin* ,Remote Sensing of Environment 100 (2006) 252 – 264

9- G. P. ASNER, 2001, *Cloud cover in Landsat observations of the Brazilian Amazon*, int. j. remote sensing, 2001, vol. 22, no. 18, 3855–3862

10- Gabriel Lellouch, Jan 2006, *Retracking of GFO satellite waveforms for inland waters studies (MSc. Thesis)*

11- Gert A. Schultz, Edwin T. Engman (Eds.), 2000, *Remote sensing in hydrology and water management.*

12- Global Reservoir Monitor (GRM), 2003, http://bigquill.gsfc.nasa.gov/, last updated Dec. 2003

13- Jens Liebe, 2002, *Estimation of water storage capacity and evaporation losses of small reservoirs in the upper east region of Ghana (Diploma thesis)*

14- *Landsat 7 Science Data Users Handbook*, 2006, Last Update December 10, 2006

15- Luis Almeida (SADC), 2004, *The keynote for introducing the main characteristics of the Incomati Basin*

16- Mather, P.M., 1999, *Computer Processing of Remotely-Sensed Images. An Introduction.*

17- Remko Scharroo, 2002, *A decade of ERS Satellite Orbits and Altimetry*

18- Rosmorduc, V., J. benveniste, O. Lauret, M. Milagro, N. Picot, *Radar Altimetry Tutorial*, 2006, J. Benveniste and N. Picot Ed., http://www.altimetry.info, 2006.

19- Sakhiwe Nkomo and Pieter van der Zaag, 2003, *Equitable water allocation in a heavily committed international catchment area: the case of the Komati Catchment*

20- Witter, D. L., and D. B. Chelton (1991), *A Geosat altimeter wind speed algorithm and a method for altimeter wind speed algorithm development*, J. Geophys. Res., 96(C5), 8853.8860.

7 Appendices

7.1 Appendix 1 - List of main current earth observation satellites (Optical)

No.	Satellite System	Year of launch	Country	Sensors	Resolution in meters & Nr. of spectral bands			Revisit	Pointing *
					Pan	Ms	Tir		
1	ALOS	2006	Japan		2.5	10 (4)		46 days	yes
2	ALSAT-1 (DMC)	2002	Algeria	DMC-MS		32(3)		4 days	
3	Aqua MODIS	2002	USA			250(2), 500(5), 1000(19)	1000(10)	2 days	
4	BEIJING-1 (DMC)	2005	China	DMC-MS / CMT	4	32 (3)			
5	BILSAT (DMC)	2003	Turkey	MS / PAN / COBAN	12	26 (4)			
6	CBERS 1+2	1999+2003	China+Brazil			20(4),80(3),260(2)	80 (1)	26 days	
7	DMC Surrey (5x)	2006-	UK			32 (3)			
8	DMSP	1972	USA			550 (2)		6 hours	
9	Envisat MERIS	2002	Europe			300 (15)		3 days	
10	EO 1	2000	USA	ALI / Hyperion	10	30(10),30(220)			
11	EROS A	2000	Israel+USA		1.8				yes
12	EROS B	2006	Israel+USA		0.7				yes
13	Fengyun 1C/1D	1999	China			1100(8)	1100(2)		
14	FORMOSAT 2	2004	Taiwan		2	8 (4)			yes
15	GMS-5	1995	Japan		1250		5000 (3)	29 minutes	
16	GOES-8,10,11,12	1994-2001	USA		1000	4000	4000(2), 8000(1)	26 minutes	
17	Ikonos 2	1999	USA		1	4 (4)		3 days	yes
18	IRS 1C/D	1995-1997	India		5.8	23.5 (4)		24 days	yes
19	IRS P2	1994	India			36 (4)		24 days	
20	IRS P3	1996	India			520 (17)	520 (1)	5 days	
21	IRS P4 (Oceansat)	1999	India			350 (8)		2 days	
22	IRS P5 (Cartosat-1)	2005	India		2.5			5 days	
23	IRS P6 (Resourcesat 1)	2003	India	AWiFS / LISS3+4		5.8(3)/23.5(4)/56(4)		5 days / 24 days	
24	KOMPSAT 1	1999	Korea		6.6	850 (6)		28 days	yes
25	KOMPSAT 2	2006	Korea/Israel		1	4(4)			
26	Landsat 4	1982	USA	MSS/TM		30 (6)	120 (1)	16 days	

No.	Satellite System	Year of launch	Country	Sensors	Resolution in meters & Nr. of spectral bands			Revisit	Pointing *
					Pan.	Ms.	Tir.		
27	Landsat 5	1984	USA	MSS/TM		30 (6)	120 (1)	16 days	
28	Landsat 7	1999	USA	ETM	15	30 (6)	60 (2)	16 days	
29	Meteosat 5	1991	Europe		2500		2500(1), 5000(1)	30 minutes	
31	MSG-1	2002	Europe	SEVIRI	1400	4800 (4)	4800 (7)	15 minutes	
32	MSG-2	2005	Europe	SEVIRI	1400	4800 (4)	4800 (7)	15 minutes	
33	MTI	2000	USA	MTI		5(4), 20(9)	20(3)		
34	MTSAT-1R	2005	Japan	JAMI	1000	4000(2)	4000(2)		
35	NigeriaSat-1 (DMC)	2003	Nigeria	DMC-MS		32 (3)			
36	NOAA-12+14	1991+1994	USA	AVHRR-2		1100 (3)	1100 (2)	0.5 day	
37	NOAA-15+16+17+18	1998+2000+2002+2005	USA	AVHRR-3		1100 (3)	1100 (3)	0.5 day	
38	ODIN	2001	Sweden	OSIRIS	1000	1000 (3)			
39	Orbview 2	1997	USA	SeaWiFS		1000 (8)		1 day	
40	Orbview 3	2003	USA		1	4 (4)		3 days	yes
41	Orbview-1	1995	USA	OTD	10000			2 days	
42	Parasol	2004	France	POLDER		7000 (9)			
43	PROBA (CHRIS)	2001	Europe	CHRIS / HRC	5	18 (18)		7 days	
44	Quickbird 2	2001	USA		0.61	2.44 (4)			yes
45	Resurs DK1	2006	Russia	ESI	1	2.5 (3)			yes
46	RESURS-01-3	1994	Russia	MSU-E+SK		34(3) / 137(4)	548 (1)	18 /5 days	
47	RESURS-01-4	1998	Russia	MSU-E1+SK1		34(3) / 210(4)	700 (1)	18 /5 days	
48	SAC-C	2000	Argentina		35	175 (5)		9 days	
49	Seastar / Seawifs	1997	USA			1100 (8), 4500 (8)		1 day	
50	SPOT 2	1990	France	HRV	10	20 (3)		4 days	
51	SPOT 4	1998	France	HRVIR / VEGET	10 (band2)	20 (3) / 1000 (4)		4 days / 1 day	
52	SPOT 5	2002	France	HRG/HRS/VEG-2	5(2.5) / 10	10(3)/20(1)/1000 (4)		5 / 26 / 1 days	
53	Terra ASTER	1999	USA	ASTER		15(3) /30(6)	90 (5)	16 days	
54	Terra MODIS	1999	USA	MODIS		250(2)/500(2)/1km(23)	500(3)/1000(6)	1-2 days	yes
55	Topsat	2005	UK		2.8	5 .6(3)		6days	yes
56	UK-DMC (DMC)	2003	UK	DMC-MS		32 (3)		daily (in DMC)	

* Pointing: Refers to the capability to focus the sensor in any direction away from the satellite path
(Source: The Netherlands National Point of Contact (NPOC): http://www.npoc.nl/EN-version/satelliteinfo/satellitetabel.html, ver.: 22-11-2006, Visited on Feb. 12,2007)

7.2 Appendix 2 - List of main current earth observation satellites (SAR)

No.	Satellite System	Year of launch	Country	SAR Resolution (m)	swath (km)	Orbit height	Revisit	Pointing *
1	ALOS	2006	Japan	10/20/100 (L-band)	35/70 | 70/250	700	46 days	Yes (ms)
2	Envisat ASAR	2002-03	Europe	30 (C-band)	60-100	800	35 days	
3	ERS 2	1995	Europe	25 (C-band)	100	780	35 days	
4	IRS P4 (Oceansat)	1999	India	7, 11, 18, 21 GHz	1420	720	2 days	
5	QuikSCAT	1999	USA	13.4 GHz	1800	803		
6	Radarsat 1	1995	Canada	8-100 (Cband)	50-500	798	24 days	Yes

* Pointing: Refers to the capability to focus the sensor in any direction away from the satellite path
(Source: The Netherlands National Point of Contact (NPOC): http://www.npoc.nl/EN-version/satelliteinfo/satellitetabel.html, ver.: 22-11-2006, Visited on Feb. 12,2007)

7.3 Appendix 3 – ERS-2 Coverage of the Incomati basin

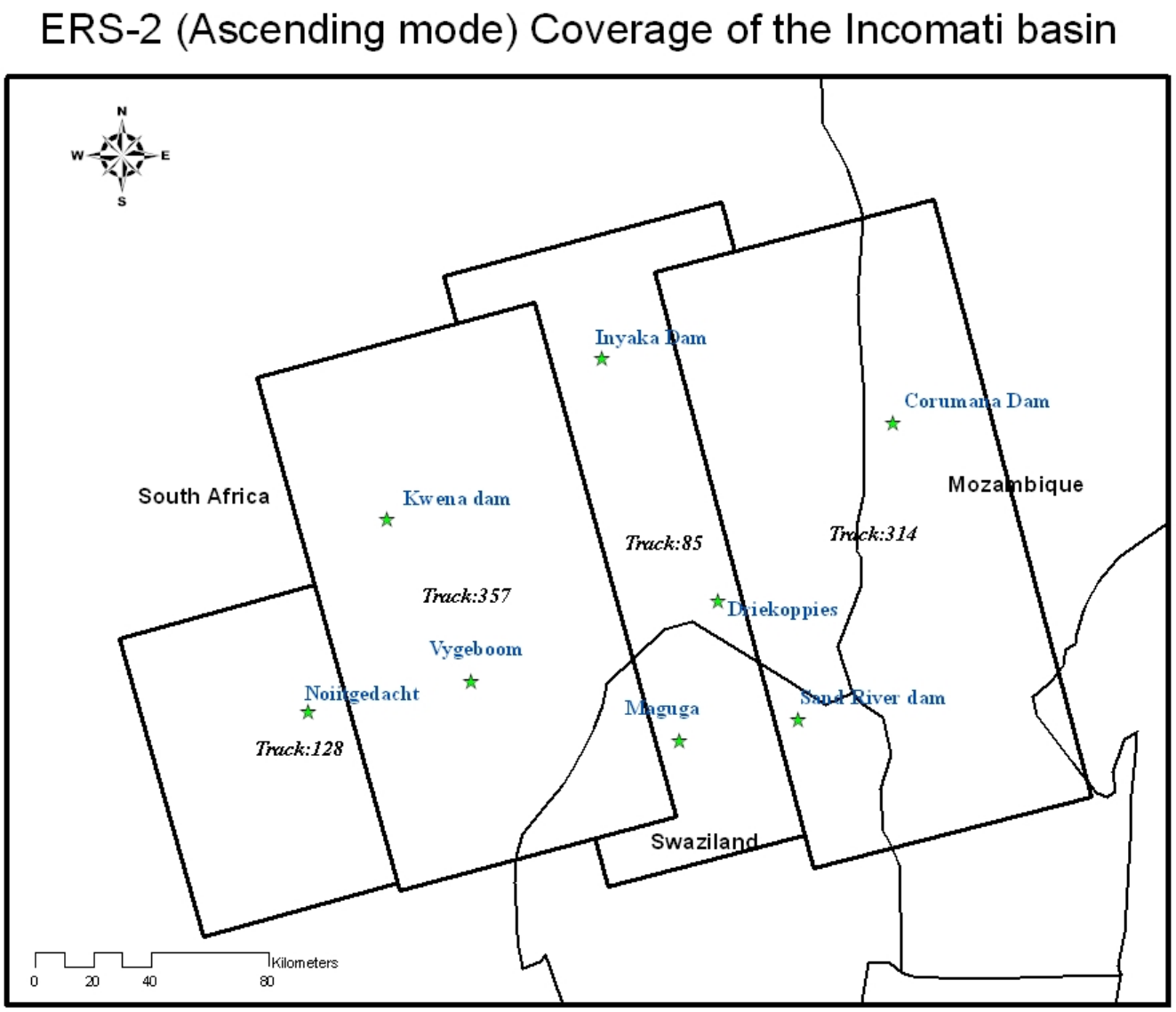

ERS-2 (Descending mode) Coverage of the Incomati basin

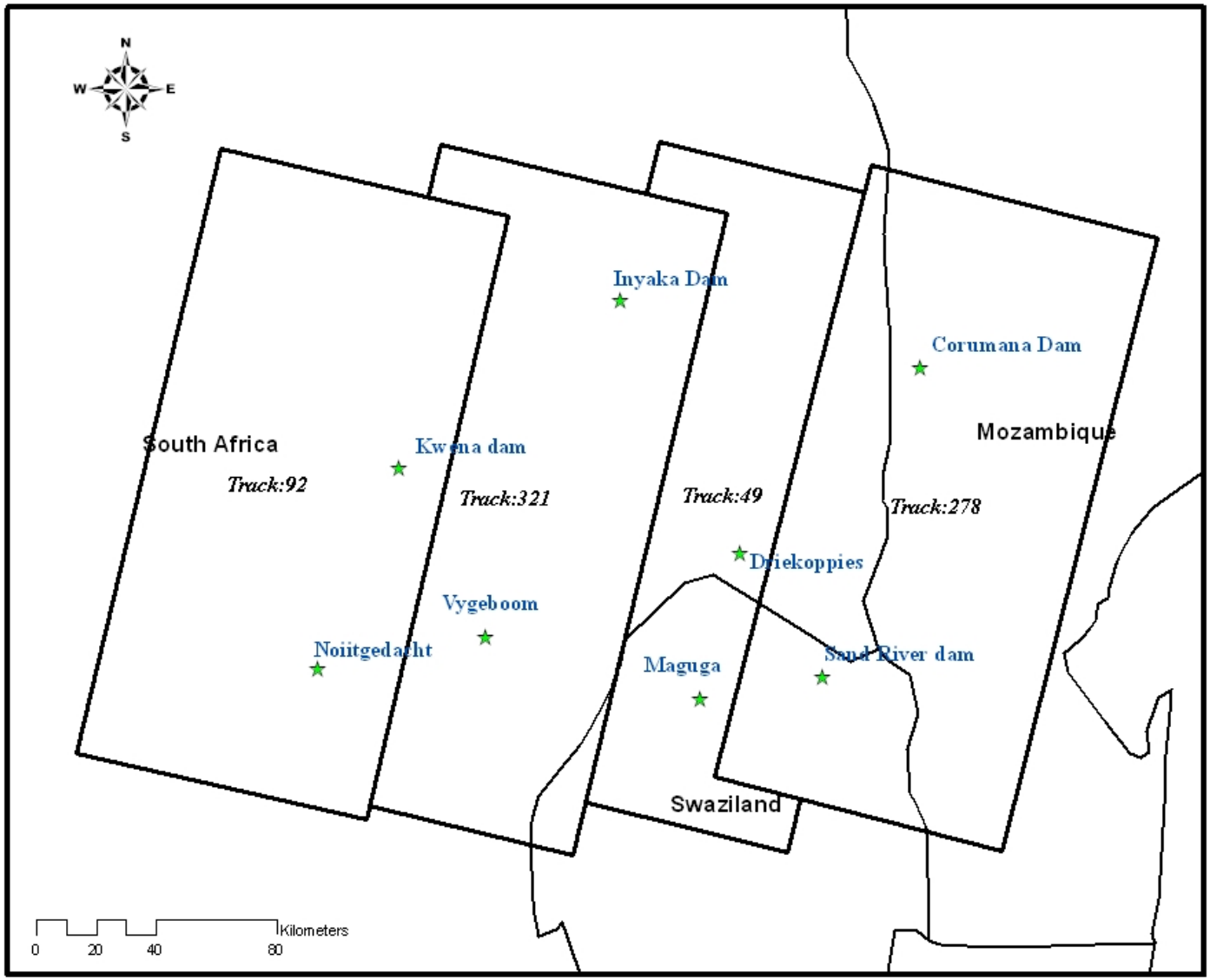

7.4 Appendix 4 – Landsat ETM+ Scene parameters

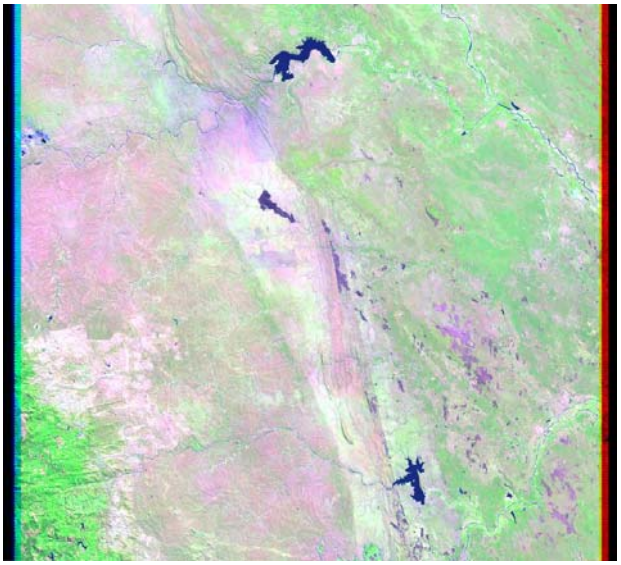

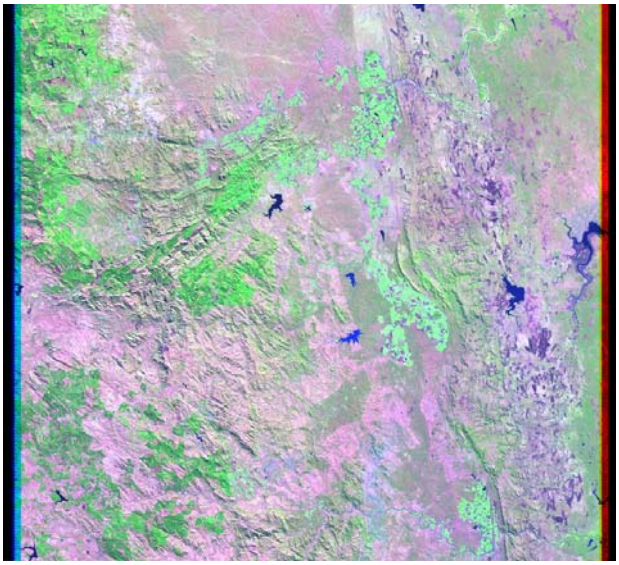

Dataset Attribute	Attribute Value
Scene ID	7168077000115050
Acquisition date	5/30/2001
WRS Path	168
WRS Row	77
Cloud Cover	0%
Day or Night	Day
Flight Path	Descending
Scene Center	24º 33' 14" S, 31º 54' 21" E
Upper Left	23º 36' 12" S, 31º 10' 12" E
Upper Right	23º 52' 24" S, 33º 2' 6" E
Lower Right	25º 30' 18" S, 32º 39' 12" E
Lower Left	25º 13' 53" S, 30º 45' 46" E
Browse available	Yes
Full / Partial	Full Scene
Sun Elevation	33.82296
Sun Azimuth	37.104057
Scene Center Time	2001:150:07:39:19.7399690

Dataset Attribute	Attribute Value
Scene ID	7168078000115050
Acquisition date	5/30/2001
WRS Path	168
WRS Row	78
Cloud Cover	0%
Day or Night	Day
Flight Path	Descending
Scene Center	25º 59' 35" S, 31º 33' 11" E
Upper Left	25º 2' 27" S, 30º 48' 37" E
Upper Right	25º 18' 50" S, 32º 41' 51" E
Lower Right	26º 56' 39" S, 32º 18' 35" E
Lower Left	26º 40' 2" S, 30º 23' 43" E
Browse available	Yes
Full / Partial	Full Scene
Sun Elevation	32.535328
Sun Azimuth	36.766003
Scene Center Time	2001:150:07:39:43.6814837

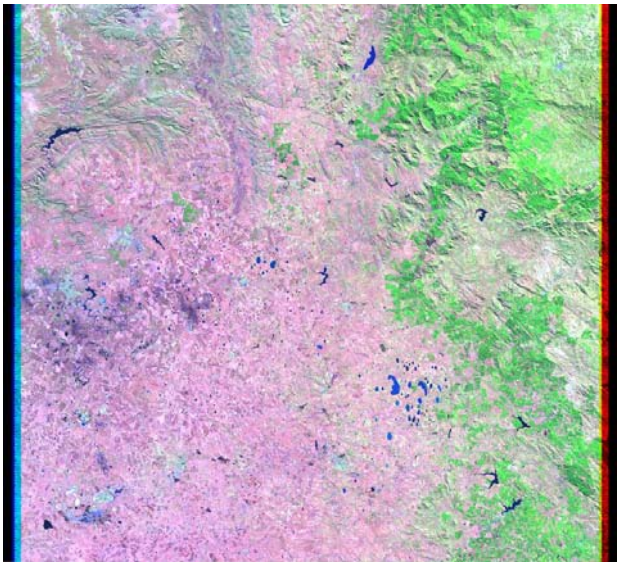

Dataset Attribute	Attribute Value
Scene ID	7169078000114150
Acquisition date	5/21/2001
WRS Path	169
WRS Row	78
Cloud Cover	0%
Day or Night	Day
Flight Path	Descending
Scene Center	25º 59' 35" S, 30º 0' 27" E
Upper Left	25º 2' 30" S, 29º 15' 50" E
Upper Right	25º 18' 53" S, 31º 9' 4" E
Lower Right	26º 56' 42" S, 30º 45' 47" E
Lower Left	26º 40' 5" S, 28º 50' 56" E
Browse available	Yes
Full / Partial	Full scene
Sun Elevation	33.952278
Sun Azimuth	37.630352
Scene Center Time	2001:141:07:45:59.5109422

Source: USGS Global Visualization Viewer (EROS)

7.5 Appendix 5 – Water level – Water surface – Water volume curves

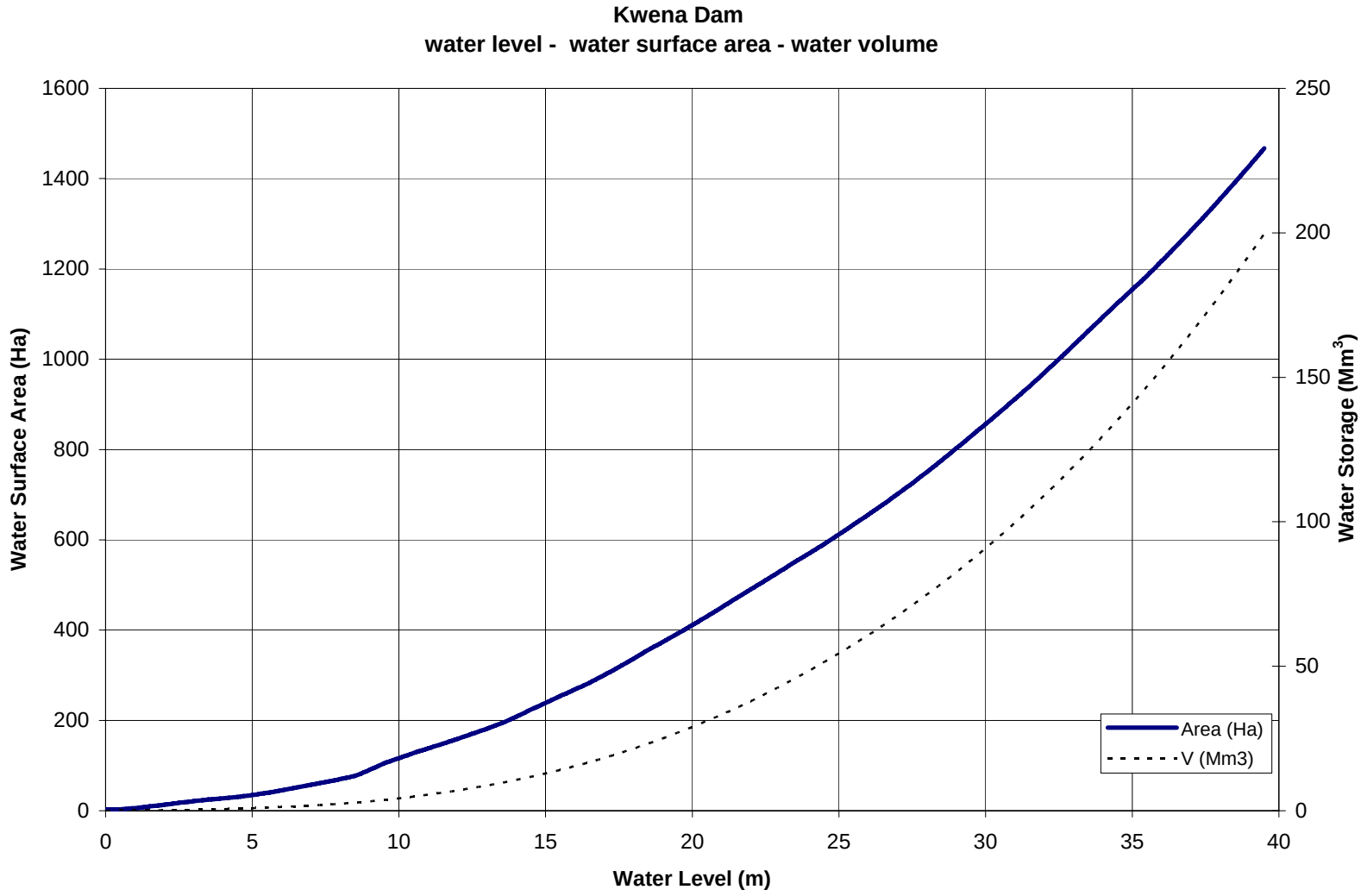

Figure 20 - Water level - Water surface area - Water volume graph for Kwena Dam. Adapted from information obtained from DWAF

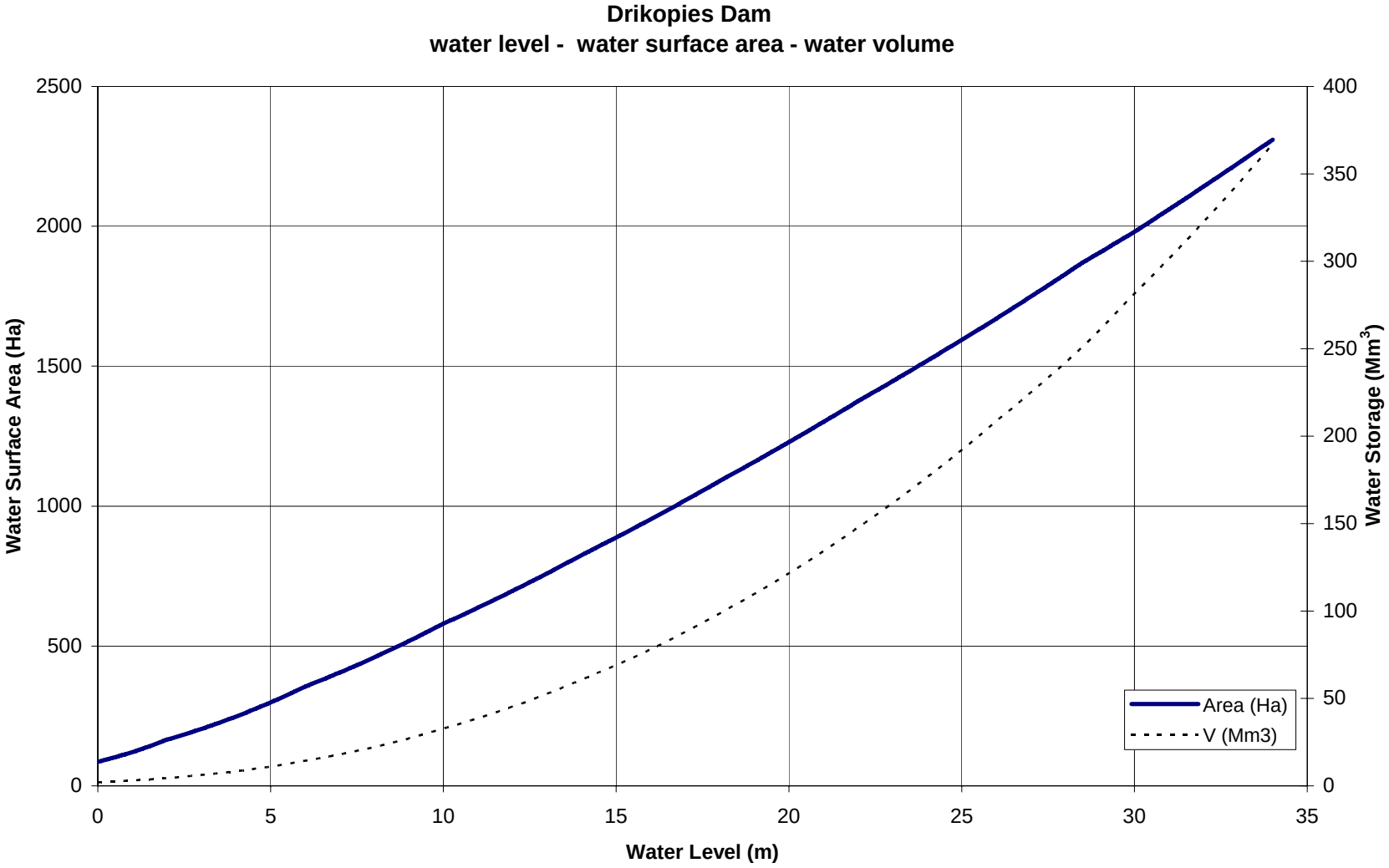

Figure 21 - Water level - Water surface area - Water volume graph for Drikopies Dam. Adapted from information obtained from DWAF

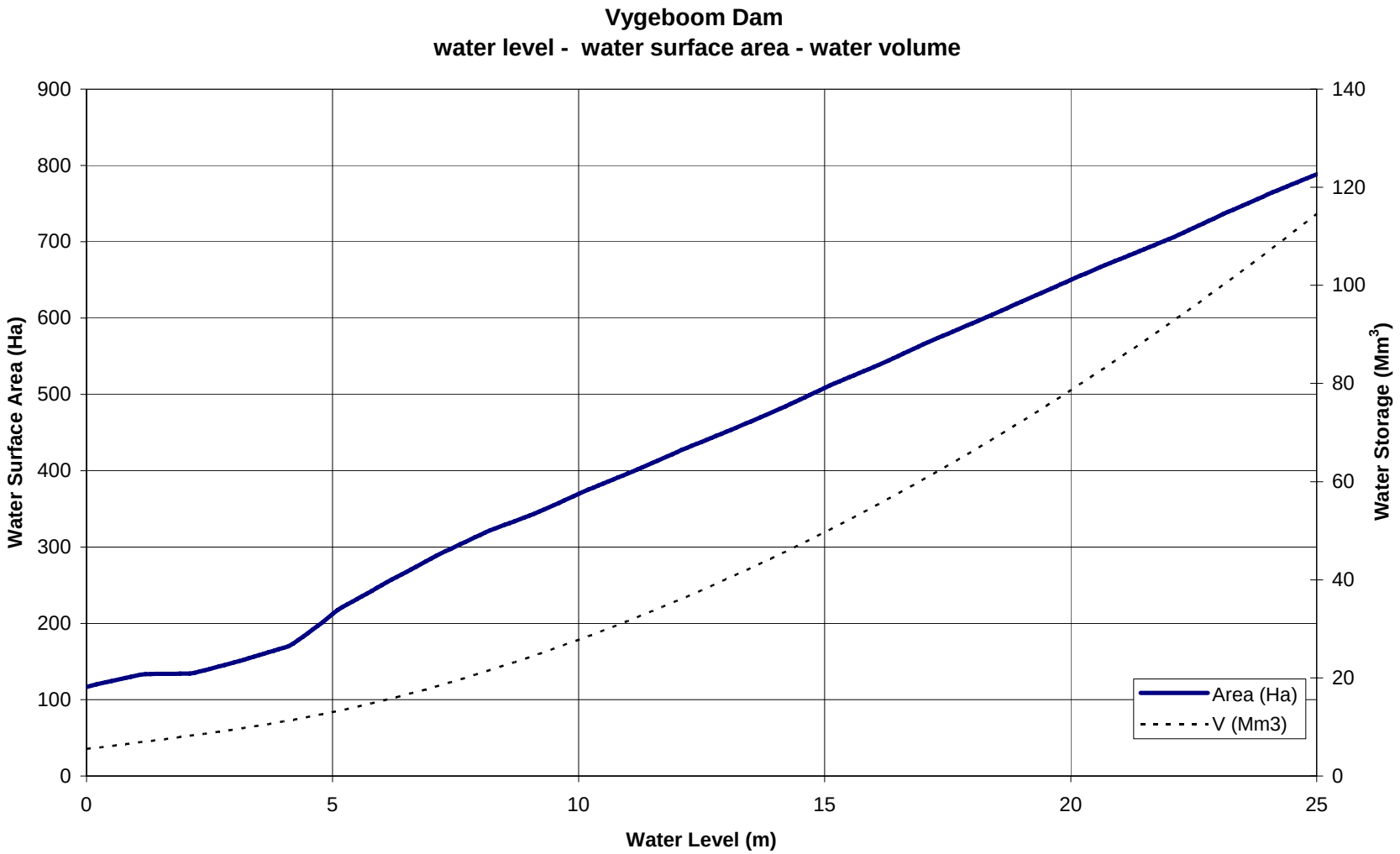

Figure 22 - Water level - Water surface area - Water volume graph for Vygeboom Dam. Adapted from information obtained from DWAF

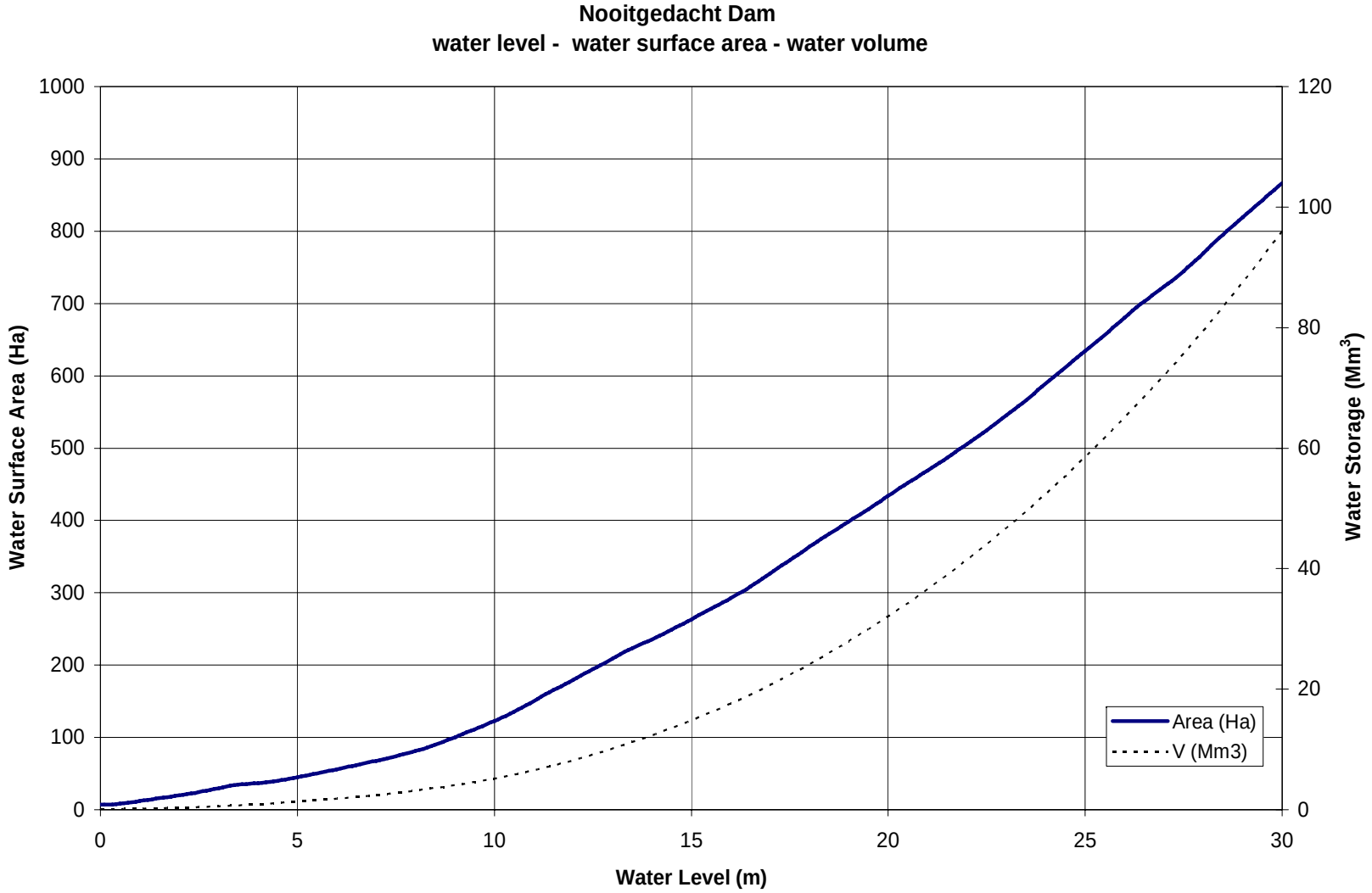

Figure 23 - Water level - Water surface area - Water volume graph for Nooitgedacht Dam. Adapted from information obtained from DWAF